Iron Oxide Nanoparticles as MRI Contrast Agents in CNS Imaging; Perfusion assessment of brain tumor therapy using ferumoxytol

PhD Dissertation

Csanád Várallyay M.D.

Semmelweis University
School of Doctoral Studies, Clinical Medicine

Supervisor: Prof. Kálmán Hüttl M.D., Ph.D.

Official Reviewers: Tibor Kovács M.D., Ph.D.
János Martos M.D., Ph.D.

Head of the Final Examination Committee:
Prof. Judit Fidy M.D., Ph.D., D.Sc.

Members of the Final Examination Committee:
Prof. Imre Szirmai M.D., Ph.D., D.Sc.
Péter Barsi M.D., Ph.D.

Budapest
2012

1 TABLE OF CONTENTS

2 LIST OF ABBREVIATIONS:

1.5T:	1.5 tesla
3D:	3 dimensional
3T:	3 tesla
BBB:	blood-brain barrier
BEV:	indicates the study group; animals treated with bevacizumab (45mg/kg)
CNS:	central nervous system
CBF:	cerebral blood flow
CBV:	cerebral blood volume
rCBV:	relative cerebral blood volume
CKD:	chronic kidney disease
CNR:	contrast to noise ratio
CT:	computed tomography
CTR:	indicates the control group; animals receiving saline
DEX 2:	indicates the study group; animals treated with dexamethasone (2mg/kg/day)
DEX 12:	indicates the study group; animals treated with dexamethasone (12mg/kg/day)
DCE:	dynamic contrast enhanced (imaging) - referring to T1w acquisition
DSC:	dynamic susceptibility contrast (imaging) - referring to T2*w acquisition
EPI:	echo planar imaging
FDA:	Food and Drug Administration
Fe:	Iron
FFE:	Fast field echo (Philips) equivalent to GRE (Siemens, GE)
FOV:	field of view
FSE:	fast spin echo (General Electric) equivalent to TSE (Siemens and Philips)
Gd:	Gadolinium
GBCA:	gadolinium based contrast agent
GBM:	glioblastoma
GRE:	gradient recalled echo (Siemens, GE) equivalent to FFE (Philips)
IF:	impact factor
IV:	intravenous
MR:	magnetic resonance
MRA:	magnetic resonance angiography

MRI: magnetic resonance imaging

MTT: mean transit time

rMTT: relative mean transit time

NSF: nephrogenic systemic fibrosis

OHSU: Oregon Health and Science University

PE-50: polyethylene 50 (tube)

PWI: perfusion-weighted imaging

r: relaxivity

$r_{1:}$ longitudinal relaxivity

$r_{2:}$ transverse relaxivity

R_1: longitudinal relaxation rate

RF: radio frequency

ROI: region of interest

SE: spin echo

SI: signal intensity

SNR: signal to noise ratio

SPIO: superparamagnetic iron oxide

SWI: susceptibility-weighted imaging

T: tesla

T1w: T1-weighted

T2w: T2-weighted

TE: echo time

T-I: time-intensity

TOF: time of flight

TR: repetition time

TSE: turbo spin echo (Siemens and Philips) equivalent to FSE (General Electric)

TTP: time to peak (in this work indicating the time elapsed between the arrival of the contrast bolus and maximum signal intensity of the enhancing tissue on dynamic T1-weighted images.)

USPIO: ultrasmall superparamagnetic iron oxide

VEGF: vascular endothelial growth factor

VSPIO: very small superparamagnetic iron oxide

3 INTRODUCTION

High-grade gliomas such as glioblastoma (GBM), anaplastic astrocytoma, and anaplastic oligodendroglioma are commonly treated with radiation therapy with concomitant temozolomide chemotherapy, followed by adjuvant temozolomide. In addition, at recurrence, as a second line therapy patients may receive anti-angiogenic therapy such as bevacizumab (Avastin®), a monoclonal antibody against vascular endothelial growth factor (VEGF) (1). Tumor response is generally determined using the Macdonald treatment response criteria, which is based on post-contrast tumor enhancement on T1-weighted (T1w) magnetic resonance (MR) images. Decreases in tumor vascular permeability and normalization of existing tumor vasculature after bevacizumab treatment (2) can be interpreted as decreased tumor volume and apparent tumor response; however, tumor progression as non-enhancing or infiltrative disease can occur in bevacizumab-treated patients (3). Bevacizumab-induced pseudoresponse, also referred to as pseudoregression, makes radiographic responses challenging to interpret. Similarly, increasing tumor vascular permeability during and after radiotherapy can result in an increasing contrast enhancement, without an increase of the underlying tumor mass, this is called pseudoprogression. Both pseudo-phenomenona confuse the assessment of outcome of brain tumours in clinical practice and in clinical trials. To overcome these issues, alternative endpoints and response criteria are needed (4).

My PhD thesis deals with a magnetic resonance imaging (MRI) contrast agent, an ultrasmall superparamagnetic iron oxide (USPIO) compound, called ferumoxytol, and its application in primary malignant brain tumors. The ultimate goal of these research projects is a “better” detection of brain malignancies, including improved specificity and sensitivity, and the evaluation of early therapeutic changes, overcoming the above mentioned issues with therapy assessment, and thus to help find the optimal therapeutic options.

This dissertation reports preclinical and clinical investigations. For better understanding, I would break the tradition and start with the clinical studies, followed by the preclinical experiments. There are two reasons justifying this; first of all, as chronologically the

clinical study was performed before, and most importantly, because results of these clinical investigations raised questions which became objectives in the preclinical experiments. The “Objectives”, “Methods”, “Results” and also “Discussion” sections are divided into two major parts, labeled as “clinical studies” and “preclinical studies”. The “introduction” discusses important features of brain tumors, focusing on MR imaging. There is a quick review of MRI itself and MR contrast agents. Also, the widely studied and still controversial treatment modality of antiangiogenic therapy will be discussed.

The nomenclature of the various iron oxide compounds can be confusing for the first time, as most of them start with “ferumox…”, such as ferumoxytol (Feraheme ®), our currently studied agent. Ferumoxtran-10 (Combidex ®, Sinerem ®) and ferumoxides (Feridex ®, Endorem ®) will also be mentioned. Throughout this work, we will often compare ferumoxytol with the commonly used gadolinium based contrast agents (GBCA). We avoid the terminology of “gadolinium” or “Gd” when referring to contrast media. GBCA will be used instead. The names of various GBCA, such as gadodiamide (Omniscan®) or gadoteridol (Prohance®) are more familiar from daily clinical practice.

3.1 Malignant gliomas

Malignant gliomas, the most common primary brain tumors, are generally highly invasive and extremely vascular tumors. Gliomas are histologically heterogeneous, with components that include varying degrees of cellular and nuclear pleomorphism, mitotic activity, vascular proliferation, and necrosis. GBM, the most malignant glioma, is the most common primary brain tumor, accounting for 12%–15% of all intracranial neoplasms. Despite decades of research and appearance of new treatment modalitites, the prognosis of GBM still remains poor (5).

3.1.1 Neovascularization in gliomas

An important factor in the malignancy of GBM is the ability of the tumor to recruit and synthesize vascular networks for further growth and proliferation. The degree of vascular proliferation is one of the most critical elements in the determination of tumor grade and prognosis for several reasons. First, the degree of vascular proliferation, or angiogenesis, is one of the most important histologic criteria (along with cellularity, mitosis, pleomorphism, necrosis) for determination of the degree of malignancy and grade of the glioma. Second, vascular networks are not only the principal route for delivery of oxygen and nutrients to the neoplastic cells and removal of metabolic waste products, such networks also serve as a path for tumor infiltration along the perivascular spaces. Third, the cerebral capillary endothelium (site of the blood-brain barrier, (BBB)) – composed of a continuous homogeneous basement membrane, numerous astrocytic processes, and tight junctions and an important host defense mechanism responsible for the regulation of movement of molecules – is frequently destroyed by malignant tumor cells. Fourth, a destroyed or altered BBB serves as a diagnostic tool at both computed tomography (CT) and MR imaging by allowing for contrast agent extravasation and, therefore, identification of the tumor (5).

3.1.2 MRI of primary brain tumors

Currently MRI is the most sensitive imaging modality in the diagnosis and follow up of brain tumors. In these patients contrast agent is given routinely, since the detection, characterization, and border delineation of the tumors need a high lesion contrast. This contrast depends on the signal differences between the lesion and the surrounding

tissue. Contrast enhanced MRI techniques allow for a better differential diagnosis, grading, therapy decision, and surgical planning, as well as providing a key parameter for follow-up imaging of tumor response to therapy (6). MRI perfusion measurement, especially relative cerebral blood volume (rCBV) measurement in tumors can be associated with tumoral neoangiogenesis. rCBV maps of glioma demonstrate not only the overall vascularity of the tumor but also the inherent heterogeneity and geographic differences within a single tumor. These CBV maps, in conjunction with conventional MR images, can be used to grade gliomas preoperatively, guide stereotactic biopsy, evaluate different tumor types, differentiate between recurrent tumor and delayed radiation necrosis, and monitor tumor response to therapy (5, 7).

3.1.3 Standard treatment of GBM

The current standard of care of high grade gliomas is surgical resection followed by radiotherapy and concomitant and adjuvant temozolomide chemotherapy. This relatively recent standard has been published in 2005 with the conclusion that the addition of temozolomide to radiotherapy for newly diagnosed GBM resulted in a clinically meaningful and statistically significant survival benefit with minimal additional toxicity (8).

3.1.4 Antiangiogenic therapy

In May 2009, the United States Food and Drug Administration (FDA) approved bevacizumab for recurrent GBM. Bevacizumab (Avastin) is a monoclonal antibody targeting VEGF, which is one of the known key regulators of angiogenesis and often overexpressed in high-grade gliomas (9). VEGF inhibitors have been successfully used in patients with high-grade gliomas (10). Along with various antiangiogenic drugs, bevacizumab has been investigated in numerous preclinical and clinical studies (11-13). Among the new biological agents, bevacizumab has been shown to induce a clinically meaningful proportion of durable responses among patients with recurrent GBM with an acceptable safety profile. Furthermore, data are emerging that bevacizumab induces improvement or preservation of neurocognitive function, suggestive of quality of life improvement, in the majority of poor-prognosis patients who would otherwise be expected to show a sudden, rapid deterioration in quality of life (14). The mechanism of these antiangiogenic agents is still not fully understood, it may include “normalization”

of existing vasculature, blocking neovascularization and decreasing edema by decreasing the BBB permeability (15).

3.1.5 Monitoring therapy – pseudoprogression and pseudoresponse

At present, the standard criteria of treatment response in gliomas are based on the GBCA enhancement (6). Tumor progression is considered to have occurred when an increase of >25% in the volume of the contrast-enhancing region is observed. Contrast enhancement, however, in post treatment brain tumors can be nonspecific and changes might not correlate with treatment response as it has been realized when introducing novel therapeutic methods. Therefore the extent of contrast enhancement may not always be considered a true surrogate of tumor response. Both pseudoprogression, an increase in the nontumoral enhancing area, and pseudoresponse, a decrease in the enhancing area, show that enhancement, by itself, is not a measure of tumor activity but rather reflects a disturbed BBB (16). Pseudoprogression can occur shortly after completion of radiotherapy; patients with high-grade brain tumors can present with an increase in contrast-enhancing lesion size, followed by subsequent improvement or stabilization without any further treatment. Pseudoresponse happens when antiangiogenic drugs act on hyperpermeable tumor blood vessels; the apparent decrease in enhancing tumor volume may represent decreased tumor vascular permeability without affecting the underlying tumor mass. This is sometimes referred to as a ‘steroid-like’ effect, as glucocorticoids are used routinely in brain tumors to decrease intracranial pressure and edema by decreasing BBB permeability. To increase diagnostic accuracy, it is critical to investigate the utility and reliability of alternative response measures, such as CBV, as measured by dynamic susceptibility contrast (DSC) perfusion MRI, and permeability, as measured by dynamic contrast enhanced (DCE) MRI (17-19).

3.2 Magnetic resonance imaging

MRI is a noninvasive technique that uses magnetic fields to produce high resolution and high-contrast sectional images of tissue structure and function. The principal tissue signal in essentially all clinical MRI arises from water protons. Water concentration can vary significantly between biological tissue. This property is exploited to produce a fundamental contrast in MRI that is known as ‘proton density contrast’. In proton density-weighted MRI, the signal intensity (SI) of each voxel is related to the local

proton concentration. Another fundamental class of MRI contrast relies on spatial differences in the relaxation properties of the MR signal. There are two principal relaxation processes that characterize MR signals: one that relates how rapidly magnetization parallel to the strong static magnetic field recovers after a perturbation, and the other that describes how rapidly magnetization transverse to the static magnetic field decays after it has been produced by a series of radiofrequency pulses. The constants that characterize these two kinetic processes are referred to as longitudinal and transverse relaxation time constants, T1, and T2, respectively. Generally, on T1w images tissues with short T1 relaxation times will appear signal intense, while on T2-weighted (T2w) images tissues with short T2 relaxation times will appear as signal loss. This will be important when discussing the relaxation time shortening effect, called relaxivity (r) of MR contrast agents.

There are numerous further parameters influencing SI. These can be exploited to obtain further image contrasts. Amongst them; the Brownian motion of water molecules in diffusion-weighted imaging, tissue blood perfusion in perfusion-weighted imaging (PWI), rapid motion of the water molecules in time of flight (TOF) MR angiography (MRA), and blood oxygenation level dependent contrast in functional MRI etc… Besides the morphology, many of these MRI techniques can reflect functional and metabolic changes.

3.2.1 High field MRI

The usual clinical MR systems operate on 1 to 3 tesla (T) magnetic field strenghts, most commonly on 1.5T. The principal advantage of MRI at higher field is the increase in signal to noise ratio (SNR). This can be used to improve anatomic and/or temporal resolution and reduce scan time while preserving image quality. Clinical MRI devices for whole body imaging at 3T are gaining wider use and a few experimental whole body 7T MR scanners are also available. Functional MRI and MR spectroscopy benefit significantly from increased magnetic field strength. In addition, high field machines have a great utility in applications such as TOF MRA and diffusion tensor imaging. Higher contrast may permit reduction of contrast agent doses and, in some cases, earlier detection of disease. Even higher field strengths can be used for imaging of small parts

of the body or scientific animal experiments. Preclinical, experimental MR scanners can reach 17.2T (Ultra-High field MRI).

For protons (hydrogen nuclei), the precession frequency of magnetic moments about an external magnetic field (Larmor frequency) is 42.58 MHz/tesla. Higher frequencies at higher field strength negatively influence the tissue penetration of radio frequency (RF) pulses, complicating the development of MR coils. The absorption of RF (microwave) power causes heating of the tissue. The energy deposited in the patient's tissues is fourfold higher at 3T than at 1.5T. The specific absorption rate induced temperature changes of the human body are the most important safety issue of high field MRI.

Tissue contrast can vary on different field strengths, as tissue relaxation is also field strength dependent. Similarly, the relaxivity of contrast agents can show substantial variations at different magnetic field strengths as discussed later.

High field MRI can be more vulnerable for imaging artifacts, such as patient movement, and also chemical shift and susceptibility dispersion increase. However, this latter one can be used for DSC PWI, which is the most common clinically relevant MR perfusion technique, and also one of the main topics discussed in this writing.

3.2.2 Magnetic properties of matter

Magnetism is a fundamental property of matter. The three types of magnetic properties are: diamagnetic, paramagnetic, and ferromagnetic. These three properties are illustrated in Figure 1.

3.2.2.1 Diamagnetism

Outside of a magnetic field, diamagnetic substances exhibit no magnetic properties. When placed in a magnetic field, diamagnetic substances will exhibit a negative interaction with the external magnetic field. In other words they are not attracted to, but rather slightly repelled by the magnetic field. These substances are said to have a negative magnetic susceptibility. Notable diamagnetic materials are: Bismuth, Silver, Carbon, Copper and water.

3.2.2.2 Paramagnetism

Paramagnetic substances also exhibit no magnetic properties outside of a magnetic field. When placed in a magnetic field, however, these substances exhibit a slight

positive interaction with the external magnetic field and are slightly attracted. The magnetic field is intensified within the sample causing an increase in the local magnetic field. These substances are said to have a positive magnetic susceptibility. Paramagnetic materials are for example: Tungsten, Aluminium, Lithium and the clinically most important Gadolinium.

3.2.2.3 Ferromagneism

Ferromagnetic substances are quite different. When placed in a magnetic field they exhibit an extremely strong attraction to the magnetic field. The local magnetic field in the center of the substance is greatly increased. These substances (such as iron) retain magnetic properties when removed from the magnetic field. Objects made of ferromagnetic substances should not be brought into the scan room as they can become projectiles; being pulled at great speed toward the center of the MR imager. An object that has become permanently magnetized is referred to as a permanent magnet (20).

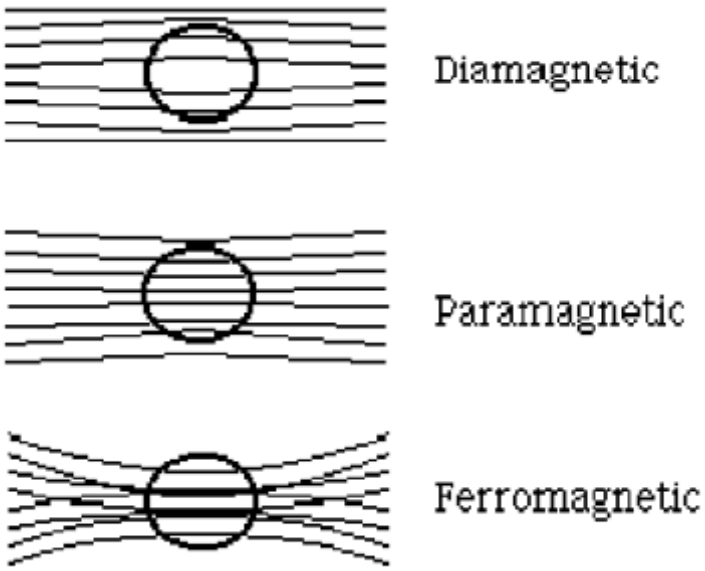

Figure 1

Schematic illustration of three types of magnetic properties of matter. Diamagnetic substances will exhibit a slight negative, paramagnetic substances a slight positive interaction with the external magnetic field, whereas ferromagnetic materials show a strong attraction to the magnetic field (20).

3.2.3 What is superparamagnetism?

Superparamagnetism is a special form of magnetism, which appears in small particles of ferromagnetic materials. In sufficiently small nanoparticles, magnetization can randomly flip direction under the influence of temperature. In the absence of external magnetic field, their magnetization appears to be in average zero: they are said to be in the superparamagnetic state. In this state, an external magnetic field is able to magnetize the nanoparticles, similarly to a paramagnet. However, their magnetic susceptibility is much larger than the one of paramagnets.

Normally, ferro- or ferrimagnetic materials undergo a transition to a paramagnetic state above its Curie temperature. Superparamagnetism is different from this standard transition as it occurs below the Curie temperature of the material.

3.3 Magnetic resonance imaging contrast agents

Although intrinsic contrast is sufficient for most MRI applications, exogenous contrast agents are used in ~40% of all clinical MRI studies. Typically, these agents are used to increase lesion conspicuity and to improve characterization of blood vessels. Unlike tracers used in x-ray or nuclear medicine imaging, MRI contrast agents are detected indirectly through their ability to catalyze water proton relaxation and perturb MRI SI. By far, the most widely used MRI contrast agents are those based on the paramagnetic gadolinium [Gd(III)] ion. The Gd(III) ion has seven unpaired electrons and favorable electronic spin relaxation properties that make for very efficient catalysis of water proton relaxation. The Gd(III) ion is chelated to a low-molecular weight ligand to reduce toxicity. After intravenous (IV) injection of these low-molecular weight GBCAs, most will distribute rapidly into all accessible extracellular spaces, and are eliminated from the body through the kidneys with a typical elimination half-life of ~1.6 h. Contrast agents catalyze relaxation rate constants (the inverse of the time constants: T1 or T2, described above) in a concentration-dependent manner. In simple solutions, the 1/T1 increases linearly with contrast agent concentration. The slope of this dependence is known as the relaxivity, typically reported in units of $mmol^{-1} sec^{-1}$, and is a measure of how potent the agent is for catalyzing relaxation. Relaxivities typically differ for longitudinal (T1) and transverse (T2) relaxation and vary with magnetic field strength. The GBCAs are typically used in combination with T1w MRI acquisitions and produce a hyperintense (bright) signal in tissue regions in which the agent accumulates. The low-molecular weight and weak protein binding characteristics of most GBCAs lead to avid extravasation of GBCAs from normal blood vessels in most tissues and abnormal blood vessels in the central nervous system (CNS). These agents have found widespread use for investigations of blood–CNS barrier disruption found in many disease pathologies (21).

3.3.1 Nephrogenic systemic fibrosis (NSF) and MR contrast agents

GBCAs in MRI are used in daily clinical practice and appear safe in most patients, however, NSF is a recently recognized severe complication associated with GBCAs. NSF is not common but can be severely debilitating and potentially fatal. It affects primarily patients with renal disease, such as stage 4 or 5 chronic kidney disease (CKD;

glomerular filtration rate of 30 ml/min per 1.73 m^2), acute kidney injury, or kidney and liver transplant recipients with kidney dysfunction. An alternative contrast agent is needed to obtain adequate imaging results while avoiding the risk of NSF in this vulnerable patient group (22).

3.3.2 Superparamagnetic iron oxide contrast agents

The superparamagnetic iron oxides are based on magnetite (Fe_3O_4) nanocrystals and are classified as superparamagnetic compounds because the net magnetic dipole moment realized exceeds that expected from the unpaired [Fe(II), Fe(III)] electrons alone. Like GBCAs, the (U)SPIOs do not retain any net magnetism once removed from the strong magnetic field; thermal energy is sufficient to destroy the net magnetic order within the nanocrystal established by the strong magnetic field. There are several imaging agents based on this construct (Table 1). The specific coating imparts differing biological properties. A complete coating protects the molecule against opsonization and endocytosis and bestows a long plasma half-life, of 14 to 30 hours (23). The utility of superparamagnetic iron oxides as MRI contrast agents has been studied for more than two decades (24) and the list of available agents is rapidly expanding (Table 1). These particles can be organized according to their hydrodynamic diameter into several categories (25): standard superparamagnetic iron oxide particles (SPIOs) (50 to 180 nm), ultrasmall superparamagnetic iron oxide particles (USPIO) (10 to 50 nm), and very small superparamagnetic iron oxide particles (VSPIOs) (< 10 nm). The USPIOs have excellent relaxivities and on a per iron-atom basis compare very favorably with GBCAs. Unlike the GBCAs, which have similar transverse and longitudinal relaxivities at clinically relevant magnetic fields, the USPIOs have significantly greater transverse relaxivities (r_2) compared with longitudinal relaxivities (r_1). The contrast effects of iron oxide agents differ across magnetic resonance sequences. On T2w MRI scans, the iron oxide agents demonstrate a decreasing signal with increasing concentration. On T1w MRI scans, ferumoxtran-10 and ferumoxytol produce a decreased signal at high concentrations and an increased signal in areas of low concentration (26, 27). For CNS imaging, T1w scans have proven to be superior for the evaluation of low concentrations of iron oxide nanoparticles across the BBB (28). Enhancement after IV infusion of feruoxtran-10 increases slowly and peaks at approximately 24 hours after

administration, then declines during the next several days (29, 30). When administered to patients with CNS abnormalities, ferumoxtran-10 allows the visualization of lesions in which the BBB is defective and/or inflammatory cells (CD68-positive macrophages or glial fibrillary acidic protein-positive reactive astrocytes) take up the particles (28, 31). Subtle defects in the BBB and inflammation may sometimes be detected more readily with iron nanoparticle agents, such as ferumoxtran-10, than with GBCAs (29). The prolonged enhancement may also be useful in comparing pre- and postoperative tumor burden and can facilitate intraoperative MRI scanning (32).

Table 1. Available superparamagnetic iron oxide agents and Prohance (Gd-based agent) for comparison

Name	Developer	Coating agent	size * (nm)	Clinical dose (µmol Fe/kg)	Relaxivity** (mM^{-1} s^{-1})
Ferumoxides AMI-25 Feridex® /Endorem®	Guerbet AMAG Pharm. Inc.	Dextran T10	120–180 (SPIO)	30	r_1=10.1 r_2=120
Ferucarbotran SH U 555 A Resovist®	Bayer Schering Pharma AG	Carboxydextran	60 (SPIO)	8–12	r_1=9.7 r_2=189
Ferumoxtran-10 AMI-227 Combidex®/Sinerem®	Guerbet AMAG Pharm. Inc.	Dextran T10, T1	15–30 (USPIO)	45	r_1=9.9 r_2=65
Ferumoxytol Feraheme®	AMAG Pharm. Inc.	Carboxylmethyl-dextran	30 (USPIO)	18–74	r_1=15 r_2=89
SH U 555 C Supravist®	Bayer Schering Pharma AG	Carboxydextran	21 (USPIO)	40	r_1=10.7 r_2=38
Feruglose NC-100150 Clariscan®	GE-Healthcare	Pegylated starch	20 (USPIO)	36	n.a.
VSOP-C184	Ferropharm	Citrate	7 (VSPIO)	15–75	r_1=14 r_2=33.4
Gadoteridol ProHance®	Bracco Diagnostics, Inc	-	1 (GBCA)	100 (µmol Gd/kg)	r_1=4 r_2=6

Currently available intravenous iron oxide nanoparticle contrast agents. Modified from (Corot, Robert et al. 2006)

* Hydrodynamic diameter, laser light scattering

** Relaxometric properties (mM^{-1} s^{-1}) at 1.5 T, 37 °C, water or in plasma; per mM Gd, or Fe.

Table 1

3.3.3 USPIO imaging at various magnetic field strength

One of the major benefits of MR imaging at higher tesla is the general gain in SNR, which can be converted into increased spatial or temporal resolution, image quality or shorter acquisition time (as mentioned previously). The assumption that the increased SNR associated with a higher magnetic field will translate into a higher contrast to noise ratio (CNR) between enhancing and non-enhancing tissue is generally true in GBCA. The effectiveness of the T1-shortening effect of a contrast agent also depends on the baseline T1 relaxation time of local tissue. With the longer baseline T1 relaxation times brought about by a higher magnetic field strength, the T1-shortening effect of GBCA will be greater, as the relaxivity of such contrast agents changes only marginally between 1.5T and 3T MRI. (34, 35). CNR increases more than two fold at higher field strength comparing 1.5T and 3T MRI using the standard 0.1 mmol/kg GBCA (36). The increased CNR allows the detection of even subtle disruptions in the BBB or could, in principle, be traded to reduce the dose of GBCA for contrast-enhanced brain imaging at 3.0 T (37).

Obviously, for T1-weigthed MRI, signal-enhancement by contrast agents is generally observed as long as the T1-shortening (caused by r_1) is the dominant effect of the contrast agent. However, a substantial T2(*)-shortening (caused by r_2), where the condition T_2(*) >>TE (TE indicates echo time) is no longer fulfilled, counteracts the signal increase in T1w contrast enhanced MRI. Hence, the achievable signal enhancement is under these conditions not only determined by the r_1, but also by r_2. Therefore, in post contrast T1w MRI larger r_1/r_2 ratios are favourable.

According to the different field strength dependencies of r_1 and r_2, generally the r_1/r_2 ratios decrease with increasing field strength. These alterations of r_1/r_2 ratios are especially pronounced for (U)SPIO (35) (Figure 2).

Similar considerations apply for T2*w MRI, such as PWI, where lower r_1/r_2 ratios can be advantageous in addition to high r_2 relaxivities (38). For this reason the use of iron oxide nanoparticles and higher magnetic field is beneficial in PWI or high resolution susceptibility-weighted imaging (SWI).

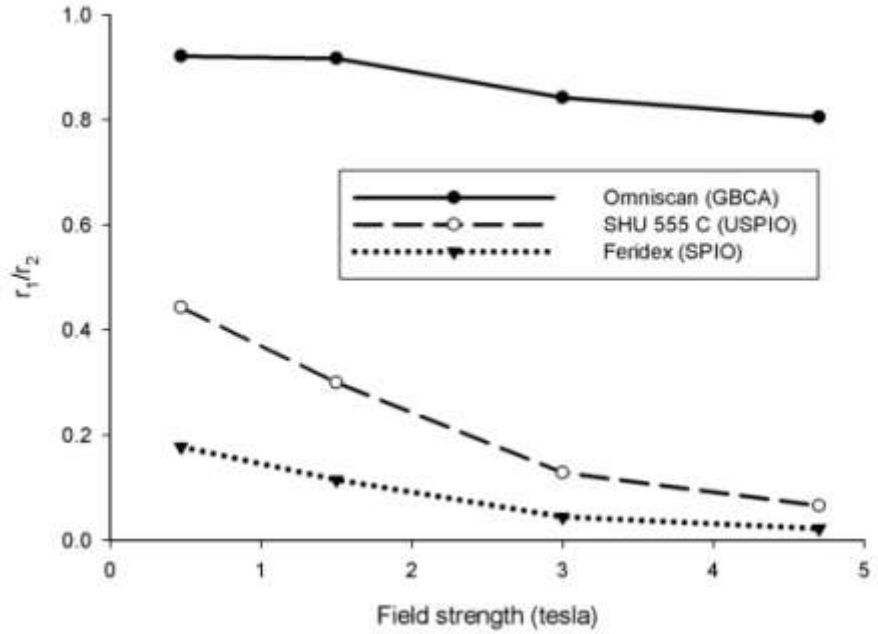

Figure 2

Field strength dependencies of r_1/r_2 ratios. Comparison of GBCA, SPIO and USPIO agents, measured at 37°C in water. (modified from Rohrer et al. (35)). GBCA displays a marginal decrease of r_1/r_2 whereas SPIOs and especially USPIOs show a considerable decrease with increasing magnetic field strength.

3.3.4 Ferumoxytol (Feraheme®)

Ferumoxytol is an ultrasmall superparamagnetic iron oxide nanoparticle approved by the United States FDA for iron replacement therapy in adults. Ferumoxytol is available for IV injection (30 mg Fe/mL) in single use vials. Each vial contains 510 mg of elemental iron in 17 mL. Ferumoxytol is also gaining utility in MR imaging. Unlike other iron oxide nanoparticle contrast agents, ferumoxytol's modified carbohydrate coating allows it to be administered as a bolus without mast cell degranulation. This property makes ferumoxytol suitable for dynamic magnetic resonance studies, such as dynamic MRA and PWI, for which it has already been used in body MRA (39, 40). Ferumoxytol particles are very large (hydrodynamic diameter ~30nm), in comparison to GBCA (~1nm). They initially remain in the intravascular space early after administration, potentially allowing PWI that is more accurate, MRA of regions with defects in the BBB (i.e., tumors), and delayed imaging to evaluate for enhancement, as

with ferumoxtran-10 (29). As an iron replacement agent, Feraheme is given in a dose of 510mg, repeated 3-8 days later. Each of these is equivalent with around 7mg/kg (in a 70kg individual). For MR imaging our study protocols usually use 2, 4 mg/kg, or a single dose of 510mg. Repeated injections are possible if they do not exceeding the therapeutic 2 x 510mg/kg doses.

3.3.5 Safety of ferumoxytol

In a prospective, double-blind, crossover study of more than 700 patients with CKD, the safety of IV bolus of 510mg ferumoxytol was studies and compared with normal saline injection. The rates of treatment-related adverse events were 5.2% and 4.5%, respectively. Serious treatment-related adverse events were seen in one patient in each treatment group. The most common adverse events with ferumoxytol occurred at the injection site (bruising, pain, swelling, erythema). Dizziness, nausea, pruritus, headache, and fatigue occurred in less than 2% of patients receiving ferumoxytol, with a similar frequency noted after administration of normal saline.

Adverse effects related to ferumoxytol were recorded in Phase 3 clinical studies of patients with CKD and iron deficiency anemia. Serious hypersensitivity reactions were reported in 0.2% (3/1,726) of subjects receiving ferumoxytol. Other adverse reactions potentially associated with hypersensitivity (e.g., pruritus, rash, urticaria or wheezing) were reported in 3.7% (63/1,726) of these subjects. Hypotension may follow Ferumoxytol administration. In clinical studies, hypotension was reported in 1.9% (33/1,726) of subjects, including three patients with serious hypotensive reactions. Excessive therapy with parenteral iron can lead to excess storage of iron with the possibility of iatrogenic hemosiderosis. (Feraheme drug insert, AMAG Pharmaceuticals, Inc. 2009)

Contraindications of ferumoxytol administarion are: evidence of iron overload, known hypersensitivity to ferumoxytol or any of its components. (41). An observation period of 30 minutes following ferumoxytol injection is recommended.

3.3.6 Pharmacokinetics of ferumoxytol

After IV injection, parenteral iron compounds distribute throughout the intravascular compartment and are slowly removed by phagocytes in the liver, spleen, and bone. Iron is released intracellularly and either stored intracellularly or can be released from the

cell and bound by transferrin in the plasma. This iron-transferrin complex can then bind to transferrin receptors on the cell membrane of erythroid precursors, and then be internalized and subsequently incorporated into hemoglobin (23). Plasma half life is around 15h. In larger doses, clearance follows nonlinear, zero-order kinetics and becomes saturable (42). There is no substantial renal elimination of ferumoxytol. Also, hemodialysis does not alter its plasma concentration.

3.4 Dynamic MRI

3.4.1 Perfusion-weighted imaging (PWI)

PWI is mostly performed using first-pass, DSC MR echo-planar imaging approaches (5). The basic principle of PWI using DSC MRI is as follows: the first pass effect of a contrast bolus in brain tissue is monitored by a series of T2*w MR images by scanning the same brain regions repeatedly. The susceptibility effect of a paramagnetic (GBCA), or superparamagnetic (SPIO, USPIO) contrast agent causes a signal loss, which can be converted into an increase of contrast agent concentration (37). From this data, parametric maps of cerebral blood flow (CBF), cerebral blood volume (CBV) and mean transit time (MTT) can be calculated. Regional CBF, CBV and MTT values can be obtained by region of interest (ROI) analysis (43).

PWI in CNS diseases have benefits for 3 major fields: improving accurate diagnosis, biopsy planning and monitoring of therapy. The higher vascularity of brain neoplasms is most commonly quantified with perfusion MR techniques in terms of the CBV of the tumor. CBV is defined as the total volume of blood traversing a given region of brain, measured in milliliters of blood per 100 grams of brain tissue (ml/100 g). CBF is defined as the volume of blood traversing a given region of brain per unit time, measured in milliliters of blood per 100 grams of brain tissue per minute (ml/100 g/min). The definition of MTT is more complex, but it can be thought of as the average time it takes for blood to traverse between arterial inflow and venous outflow, measured in seconds (s). MTT will therefore depend on the path taken by the blood to travel from artery to vein, and as such will depend on local tissue hemodynamics, such as shunts and vessel tortuosity. The concepts of CBF and MTT have not been as fully studied in the context of oncologic imaging as has CBV, despite their widespread application in stroke imaging (5, 44, 45).

3.4.2 Issues with CBV calculation

Using the DSC technique, CBV is estimated from the area encompassed by the time - intensity curve, which is inverted in this case, since there is signal loss. DSC PWI is based on the premise that contrast material remains within the intravascular compartment. High permeability or leakiness in regions of marked breakdown of the BBB results in intravascular gadolinium extravasating into the interstitial space. Extravasation can significantly affect calculations and alter CBV values (46). and this could lead to false results in monitoring tumor therapy especially when primarily microvasculature is targeted (e.g. antiangiogenic therapy). Several methods have been used to correct, or more appropriately, compensate for the unwanted effect of extravasation on rCBV calculations, including mathematical algorithms, such as excluding portions of the SI time curve from the calculations. This corrective method still leads to underestimation of the rCBV. Another method, sloping baseline, leads to artifactually high rCBV. One of the most common contrast material extravasation correction methods is administration of a loading dose of GBCA before DSC PWI acquisition. This is referred to as the "preload method". This could increase the diagnostic accuracy, however it seems to be dose-dependent and was found to be inconsistent in longitudinal studies assessing antiangiogenic treatment (47). Therefore the use of a blood pool agent (such as the bolus injectable USPIO ferumoxytol, or SHU 555 C) would be favorable by eliminating the permeability dependence of CBV estimation. Furthermore due to its more effective T2 relaxation time shortening (r_2), a more pronounced signal drop can be reached without the need of injecting large contrast bolus volumes with a high flow rate.

3.4.3 DCE permeability measurement

The angiogenic process is heterogeneous within tumors, with some vessels demonstrating maturity and other vessels demonstrating incomplete layers with high permeability and fragility. Angiogenic vessels in the tumor have large gaps between the endothelial cells, the endothelium, and the basement membranes, as well as between the basement membrane and the pericytes, making the vessels hyperpermeable to many macromolecules. These properties can be exploited by DCE-MRI. MR contrast agents that leak slowly through the normal vasculature are able to pass more quickly through

tumor vessels to produce differential enhancement. This results in a fast “wash-in” of contrast coupled with the rapid “wash-out,” and allows a functional analysis of the tumor microcirculation (48). DCE-MRI is performed by repeated (dynamic) T1w imaging of tissue started immdiately after injection of low-molecular-weight contrast media. If a reliable arterial input function (AIF) can be obtained, the rate of contrast agent leakage can be quantified. Tofts et al (49) proposed the terms volume transfer constant (K^{trans}) (min^{-1}), the volume of extravascular extracellular space (EES) per unit volume of tissue (v_e) and the flux rate constant between EES and plasma (kep) (min^{-1}) as outcome parameters derived from a two-compartment general kinetic model, which is the most widely accepted model. There are numerous publications using a newer, three-site equilibrium water exchange model (50).

4 OBJECTIVES

4.1 Clinical studies:

Ferumxytol has not been used before as an imaging agent in the CNS. The clinical objective of my work was to investigate the potential for this USPIO as an MR contrast agent in CNS malignancies:

1. Evaluation of enhancement time course, and comparison with standard GBCA enhancement on T1w scans.
2. Assessing the utility of ferumoxytol in various MR imaging techniques, such as T2* weighted imaging, TOF MRA and PWI, using the DSC technique.
3. Comparison of MR imaging using ferumoxytol at various magnetic field strengths.

4.2 Preclinical studies

My further research with ferumoxytol was focused on standardized preclinical experiments, allowing a more objective assessment of this iron oxide compound in dynamic PWI of brain tumors using a 12T experimental MR system. The ojectives were:

4. To develop a study protocol, including an intracranial tumor model in rats, and serial dynamic MR imaging at 12T with bolus injection of ferumoxytol and GBCA.
5. Comparison of dynamic imaging using ferumoxytol vs. GBCA.
6. Detection of early therapeutic changes of the antiangiogenic drug, bevacizumab, using a dual agent MR imaging method (ferumoxytol for perfusion assessment and GBCA for permeability estimation)

5 METHODS

5.1 Clinical studies

The clinical data presented in this work is derived from an imaging study, which has been completed and published (33). The study was sponsored by the National Cancer Institute and approved by the FDA and the Oregon Health & Science University (OHSU) institutional review board.

5.1.1 Patients

The study consisted of 12 patients with primary or secondary brain malignancies. All patients provided written informed consent before enrollment in the study. Laboratory tests were performed within 14 days before entry in the study. Patients who were pregnant, younger than 18 years old, had a known allergy to the contrast agents, or had hemochromatosis, liver function insufficiency, or uncal herniation were excluded. No chemotherapy or other treatments were administered to the patients between the time of the baseline scan and the ferumoxytol infusion. Patients underwent multiple MRI scans as Figure 3 describes.

5.1.2 Imaging

5.1.2.1 Contrast agents used in the study

Gadodiamide (Omniscan; GE Healthcare AS, Oslo, Norway) was used in all scans in which GBCA was required in a dose of 2 x 0.1mmol/kg. The investigational agent ferumoxytol (Advanced Magnetics, Inc., Cambridge, MA) was provided by the manufacturer. Ferumoxytol was injected in total 4mg/kg (1mg/kg undiluted (~2ml of the 30mg/ml solution) as a bolus for dynamic imaging, and the rest 3mg/kg was administered diluted)

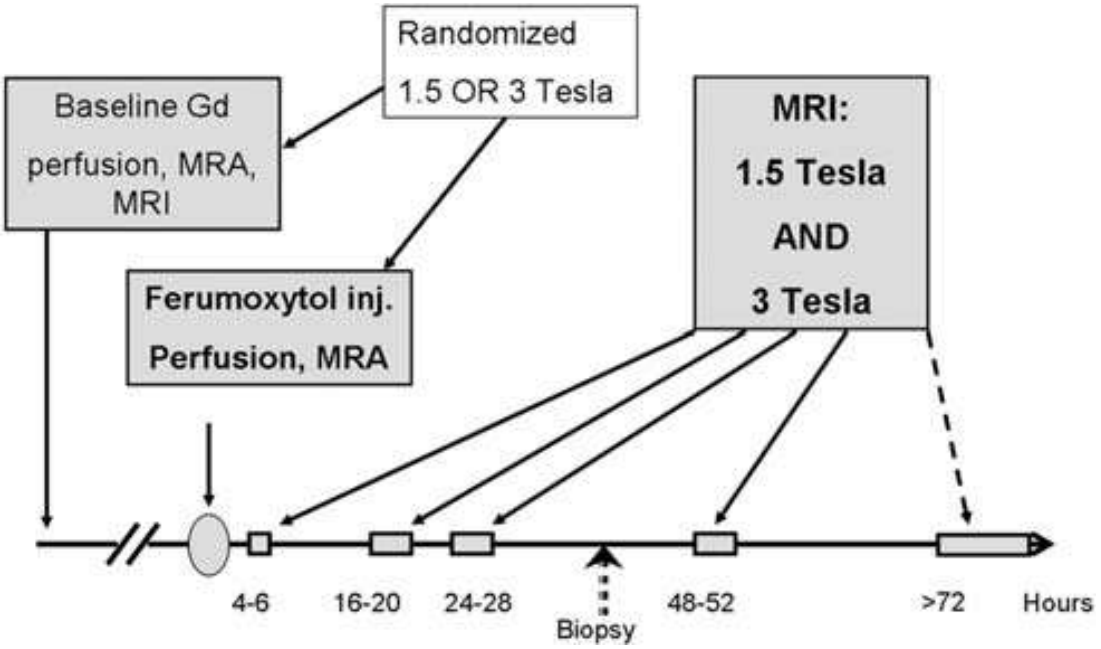

Figure 3

Imaging schedule; each patient had an initial MRI scan with and without gadodiamide. Patients were randomized to a 1.5T MRI (Horizon LX; GE Medical Systems, Milwaukee, WI), or to a 3T MRI (Intera; Philips, The Netherlands) for the initial and for the subsequent dynamic scans. Delayed MRI scans were obtained at 4 to 6 hours, 16 to 20 hours, 24 to 28 hours, 48 to 52 hours, and longer than 72 hours after infusion for each patient on both 1.5- and 3T magnets.

5.1.2.2 Ferumoxytol enhancement time course

To evaluate delayed contrast enhancement with ferumoxytol, MRI scans were obtained at 4 to 6 hours, 16 to 20 hours, 24 to 28 hours, 48 to 52 hours, and longer than 72 hours after infusion for each patient on both 1.5- and 3T magnets using standard T1w, standard T2w, T2*w axial scans (Figure 3). To analyze the changes in ferumoxytol enhancement in tumor and normal tissue, the baseline noncontrast T1w and all post-ferumoxytol T1w scans for each patient were aligned to the baseline scan via a semiautomated coregistration technique implemented using BrainVoyager QX (Brain Innovations BV, Maastricht, The Netherlands). In each patient, a tumor ROI and an ROI of normal apperaring brain tissue were defined and applied to the coregistered scan. ROIs of enhancing lesions were defined using a semiautomated method. The control ROIs were used to correct for changes in SI in healthy tissue, resulting from fluctuation

in scanner sensitivity across time and nonspecific enhancement in normal tissue, using a custom program implemented in Mathlab7 (Mathworks). For each field strength, the time of the maximum SI on T1w images was determined in each patient and the average of the relative SIs was plotted as a function of time. Data from patients with intervening surgery were not included after surgery because of changes in SI that may be caused by blood products in the operative field (51, 52). Five patients had additional imaging performed with a low-field 0.15-T intraoperative MRI scanner (Polestar N10 or N20; Medtronic, Louisville, CO) during surgery 24 to 48 hours after ferumoxytol administration. T1w axial sequences using preset standard parameters provided with the system were obtained intraoperatively. The extent of the enhancement was estimated bidimensionally. On representative slices, the largest diameter was averaged by its perpendicular diameter and plotted as a function of time. For qualitative analysis, ferumoxytol enhancement was compared with gadodiamide by the same unblinded reviewers. The regional correlation of enhancement, the enhancement characteristics, and intensity were noted.

5.1.3 TOF MRA and T1 measurement

TOF MRA (n=6) and T1 measurement (n=5) was performed in patients randomized to the 3T MRI for dynamic imaging. Quantitative T1 measurement was permormed before and within 20 minutes after contrast administration in order to detect subtle contrast agent extravasation early after injection. T1 values were obtained in ROIs of the tumoral, peritumoral, and control areas using a multishot "Look-Locker" imaging sequence for five patients. The regional uptake of contrast agent can be assessed quantitatively by T1w changes, independent of any other effects such as T2w changes, and magnetic susceptibility-related signal changes. The longitudinal relaxation rate (R_1=1/T1) changes in linear proportion to the local contrast agent concentration in blood and tissue (53, 54). The values of R_1 in the enhancing lesion and the peritumoral region were normalized by the R_1 value in a remote control area to assess the differential contrast between lesions or lesion periphery. Similarly TOF-MRA was performed before and 15-20 minutes following contrast agent administration. Images were assessed visually comparing images without contrast, with gadodiamide or with ferumoxytol.

5.1.4 Dynamic MRI scans

DSC scans were performed either at 1.5 or 3T. Three patients underwent 1.5T dynamic MRI scans and the remainder underwent 3T dynamic MRI scans. For perfusion evaluation, ROIs of the enhancing tumor and peritumoral area (surrounding abnormal T2w signal areas) and in control areas (normal appearing white and/or gray matter) were chosen by one of the authors (CGV) (55). Time-intensity (T-I) curves, CBV parametric maps and rCBV values (56) (as the area under the SI) curve, normalized by the area under the curve for the control region) were obtained using a dedicated workstation (Advantage Windows 4.2. with Functool software; GE Healthcare, Milwaukee, WI). Relative MTT (rMTT) values were obtained by γ-variate fitting the T-I curves (57), using the Mathlab environment (Mathworks, Natick, MA).

5.1.5 MRI acquisition parameters

All MRI scans were acquired with a field of view (FOV) of 230 to 240 mm (unless otherwise indicated) using 3-mm thick contiguous in the axial plane and 5-mm thick slices with a 1-mm interslice gap in the sagittal plane.

5.1.5.1 1.5-Tesla unit:

MRI acquisitions included T1w sagittal spin echo (SE) images with a repetition time (TR) of 500 ms and an echo time (TE) of 9 ms, T1w axial SE images with a TR of 600 ms and a TE of 20 ms, T2w axial echo planar imaging (EPI)- SE images with a TR of 4000 ms and a TE of 91 ms, T2w axial EPI gradient recalled echo (GRE) images with a TR of 550 ms, a TE of 23 ms, and a flip angle of 10 degrees), PWI EPI-SE images with a TR of 2600 ms and a TE of 80 ms, 1 image/s matrix 64 x 64.

5.1.5.2 3-Tesla unit

Scans were optimized for 3T, including T1w sagittal SE images (TR, 525 ms; TE, 10 ms), T1w axial turbo spin echo (TSE) images (TR, 700 ms; TE, 7.2 ms; TSE factor, 3), T1w axial fast field echo (FFE) images (TR, 150 ms; TE, 2 ms; flip angle, 80 degrees), T2w axial TSE images (TR, 3000 ms; TE, 80 ms; TSE factor, 15), T2w axial FFE images (TR, 1534 ms; TE, 16 ms; flip angle, 18 degrees), PWI EPI (TR, 35 ms; TE, 28 ms), 1 image/s, matrix 128 x 128., three-dimensional TOF MRA: GRE (TR, 14.7 ms; TE, 2.4 ms; flip angle, 20 degrees; FOV, 250 mm; matrix, 1024 x 1024; slice thickness,

0.5mm), and quantitative T1 measurement (segmented GRE cine with nonslice selective inversion pulse (TR, 6.3 ms; TE, 3 ms; flip angle, 10 degrees; matrix, 240 x 200; slice thickness, 280 mm) sequences.

5.1.6 Statistical analysis

In DSC PWI studies for statistical analyses, Student's t tests were used to determine the significance of the quantitative perfusion parameters. Unpaired t-tests compared the enhancing region and the surrounding non-enhancing area with abnormal T2w signal and paired t-tests compared the same ROIs with ferumoxytol versus GBCA.

In quantitative T1 measurement, R_1 values before and after contrast were compared via the linear mixed effects model to account for correlations between repeated measurements (with gadodiamide and ferumoxytol) in the same subject.

5.2 Preclinical studies

5.2.1 Tumor model

The U87 human glioma intracerebral xenograft model was selected for the study because it is known to be a vascular tumor that overexpresses VEGF (58) and has previously been used to study antiangiogenic treatment response (59). U87MG human glioma cells were cultured in Dulbecco's Modified Eagle's medium supplemented with 10% fetal bovine serum and antibiotics. The care and use of animals was approved by the Institutional Animal Care and Use Committee and were supervised by the OHSU Department of Comparative Medicine. Male athymic nude rats (rnu/rnu, 252 to 332 g; from the OHSU BBB Program in-house colony) were anesthetized with intraperitoneal ketamine (60 mg/kg) and intraperitoneal diazepam (7.5 mg/kg). Because of previous inconsistencies of this tumor model, all rats were treated with cyclophosphamide (300mg/m^2 i.p.) 24 h prior to tumor implantation to increase tumor growth (60). Animals received 1.2 to 1.5 * 10^6 of > 90% viable U87MG cells in a volume of 15µL, stereotactically injected in the right caudate nucleus (vertical, bregma 5 mm; lateral, bregma 3 mm). The needle was initially advanced to a depth of 6.5 mm and then withdrawn to a depth of 5 mm to limit reflux up the needle track. The animals were examined daily and weighed at least weekly. Animals were sacrificed if they showed severe clinical signs or symptoms, or > 20% weight loss. Tumor growth was monitored weekly using MRI starting 14 days after implantation. Studies were started when tumor volumes reached at least 50 mm^3. Animals without tumor growth were sacrificed at week 7.

5.2.1.1 Histology

After animals had to be sacrificed the brains were excised and fixed in 10% buffered formalin for vibratome sectioning at 100 µm in the coronal plane. Histology sections were stained with hematoxylin. For USPIO localization, iron histochemistry was performed using the Diaminobenzidine-enhanced Perl's stain (26).

5.2.2 Animal preparation for MRI

5.2.2.1 Sedation for MRI

When performing serial MR imaging in rats, especially in intracranial tumor bearing rats, one of the major issues is the anesthesia. The intraperitoneal ketamine – diazepam combination, which was used for tumor inoculation appeared to be unsafe in our tumor bearing animals. Overdosing caused cardio-respiratory insufficiency and death, insufficient doses caused substantial motion artifacts. Therefore (except for the first few animals) in the current study an other drug, medetomidine (0.6 mg/kg, Domitor, Pfizer Animal Health, Exton, PA, USA) was applied intraperitoneally, combined with reduced dose of ketamine (15mg/kg). This resulted in a 1 to 2 hour long motionless deep sedation. After the MRI, medetomidine was reversed using 1 mg atipamezole (Antisedan, Pfizer Animal Health, Exton, PA, USA).

5.2.2.2 Preparing the animals for contrast agent injection

Dynamic contrast studies need a reliable venous access for rapid bolus contrast agent injection followed by a saline flush. It could be problematic in small animals as the number of available veins is limited. Many studies use the tail vein. This needs a preparation before each imaging session. Tail veins of our animals were small, and veins were needed at least 4 times on four consecutive days with a relatively high flow rate, therefore we did not decide on tail vein injection. Another possibility would have been the femoral vein. Although it requires a minor surgery with a skin incision above the vessel, femoral vein is often used for IV contrast agent imaging, or applying continuous anesthesia.

For our study we decided on a third method. A catheter in the external jugular vein was placed surgically prior to the first MRI session. This was performed under surgical stereo-microscope. After preparing the vessel, its distal part we occluded with a tight suture. Proximal from this suture a small longitudinal incision was made using micro scissors, and a sterile Polyethylene 50 (PE-50) tube was inserted into the vein and advanced 1 to 2 cm toward the heart. After tightening the catheter around the vein, it was tunneled subcutaneously to the back of the animal, and fixed to the skin. The skin incision on the neck was sutured. This catheter could be used for dynamic contrast (DCE and DSC) MR imaging. After each imaging session, jugular catheters were

flushed with 0.5ml of heparinized saline (5 to 50 U/mL), and then sealed by heat, and were preserved under the back skin for the dynamic MR session the next day. Drugs for tumor treatments (e.g. bevacizumab, see later) were applied through this catheter too. Animals with jugular catheters were kept in separate cages.

5.2.3 MR imaging at 12T

Animals with jugular catheters were placed in the 12T MRI scanner (Bruker, Billerica, MA, USA). Throughout MR scans, warm water was circulated under the animals to keep them warm, and oxygen saturation and heart rate were monitored. A 7-cm quadrature birdcage coil was used to transmit radiofrequency, and a 2-cm surface coil, placed on the animal's head, was used to receive radiofrequency. Both coils were actively decoupled. High-resolution anatomical T2w scans were performed in both the coronal and axial planes for accurate planning of dynamic MR imaging (DSC and DCE studies). TR: 1560ms, TE: 21.3ms, echo train: 8, FOV: 2.3 x 2.4 cm^2, matrix 192 x 392.

5.2.3.1 Technical issues with contrast bolus delivery

Standardization of the injected contrast bolus was crucial for reproducibility. This however posed problems for the following reasons: The infusion pump had to be placed outside of the magnet room, due to the high magnetic field strength, and the distance between the infusion pump and the animal was long, measuring more than 4 meters. Also, relatively small volumes had to be injected (60µl of contrast agent), with a constant flow rate.

To ensure precise delivery, the end of the catheter was preloaded with contast agent. The injected volume of 60µl was equivalent to 22 cm of the PE-50 Tube. The dark brown color of ferumoxytol made this measurement simple. The transparent gadodiamide (Omniscan) contrast agent was stained with a small amount of Ewans blue for easier differentiation from saline. Proximal and distal from this preloaded contrast agent, the tubes were filled with saline. The mixing of the saline and contrast agent could be prevented by allowing a minimal air bubble in both ends of the contrast bolus in the PE-50 tube.

To provide a consistent flow rate we used an infusion pump. The distance between the pump and the animal was first bridged using a saline filled PE-50 (very thin and flexible) tube. Due to the high resistance, and distensibility of this tube the contrast

bolus administration became delayed and the bolus stretched out, the flow rate became inconsistent and has also decreased. A viable solution overcoming this issue was the use of 3 human perfusion tubes (with larger inner diameter) connected together and filled up with saline and connected at one end to the injector, and on the other end to the PE-50 tube which was previously filled with contrast agent. This rigid system provided a better coupling between the infusion pump and the animal. The contrast bolus remained short as planned.

5.2.3.2 Dynamic MR imaging parameters

In this work the following terminology is used. DSC imaging will indicate a T2*w rapid acquisition. The main purpose of this scan type is to obtain a signal drop as the bolus contrast passes the brain. This technique is used for brain perfusion measurement. The DCE technique will indicate a T1w rapid image acquisition. Primarily the BBB permeability of a contrast agent can be studied. High permeability will result in a rapid and intense positive enhancement peak after contrast administration.

For the DSC gradient echo images, the following parameters were used: TR 9.7 ms, TE 4.0 ms, flip angle 51, slice thickness 1.4mm, rectangular FOV 3.6 * 2.6 cm^2, 128 read-out points, and 64 phase encode lines, zero filled to 128 lines. These resulted in a 0.6-sec per image time-resolution and an in-plane (zero filled) spatial resolution of 280 μm * 200 μm. During this, rapid single slice coronal T2*w image acquisition, 60μl of undiluted contrast agent was injected as a short bolus using an infusion pump, followed by a saline flush of 240 μl at a 3 ml/min flow rate.

DCE was performed using 60μL of preloaded, twofold diluted (250mmol/l) gadodiamide bolus (Omniscan, GE Healthcare, Waukesha, WI, USA) followed by 240 μl saline flush administered at a 1 ml/min flow rate during rapid repeated single-slice T1w image acquisition. For these DCE gradient echo images, the following parameters were used: TR 25.0 ms, TE 1.7 ms, flip angle 20, slice thickness 1.0 mm, rectangular FOV 5.1 x 2.6 cm2, 128 read-out points, and 64 phase encode lines. These resulted in a 1.6-s per image time-resolution, and an in-plane (zero filled) spatial resolution of 400 μm * 400 μm. Inflow saturation slices, having a thickness of 3.0mm and a gap of 1.0mm from the slice of interest, were applied both anterior and posterior to the slice of interest.

5.2.4 Ferumoxytol vs. gadodiamide in MR perfusion and permeability

Before testing antiangiogenic treatment, two U87 tumor-bearing animals were used to test the feasibility of the study, comparing ferumoxytol and gadodiamide injections in both DSC and DCE MRIs. Animals underwent contrast enhanced T1w scans, on the first day using gadodiamide and one day later with ferumoxytol. These sequences were the same as used for DCE imaging in our further studies.

For DSC imaging we expected, that the rapid extravasation of the small molecular weight gadodiamide will influence the perfusion measurement in this high permeable tumor model. To prove this hypothesis tumor bearing animals underwent DSC PWI using a 60µl undiluted (0.5mmol) gadodiamide. 24h later, when gadodiamide was virtually eliminated, the same study was repeated with the same volume of undiluted ferumoxytol (30mg Fe/ml). T-I curves were analyzed and CBV perfusion maps compared.

5.2.5 Study design for monitoring antiangiogenic treatment

After completing these feasibility experiments and solving the technical issues, we were ready to start the study of monitoring antiangiogenic treatment. We used serial dynamic contrast MRI (DCE and DSC) at 12T to assess vascular responses to antiangiogenic therapy. Our clinical experiences with bevacizumab (Avastin®) showed rapid edema decreasing effect in patients with high-grade glioma, similar to high dose corticosteroids, therefore as a control also corticosteroid treated animals were scanned.

Athymic rats with intracerebral U87MG human glioma (n = 17) were included in the study. Five animals received bevacizumab (45 mg/kg) as a single IV injection (through the jugular catheter) in a volume of ~0.6 mL ("BEV" treatment group). Four animals were treated with a standard animal dose of dexamethasone (2 mg/kg per day, intramuscularly, twice a day) (61), this group was labeled as "DEX 2". Five animals received a higher dose of dexamethasone (98 mg/m^2 per day, intramuscularly, twice daily) (62), equivalent to 12 mg/kg per day in a 300 g rat, therefore this group was labeled as "DEX 12". Three control (CTR) animals received saline only.

5.2.5.1 Dual agent imaging

In this study both contrast agents (ferumoxytol and gadodiamide) were applied in each imaging session (dual agent imaging) for the following reasons:

Once the tumor reached the minimum of 50mm^3 due to its rapid and aggressive growth, the dynamic imaging study had to be completed as soon as the MR schedule allowed it. For similar considerations, due to this rapid tumor growth we were only able to detect short-term changes after therapy; there was no time to separate the DSC imaging using ferumoxytol and DCE with gadodiamide. This has been a major difference compared to our prior clinical protocols, in which at least 24 hours had to pass between the two contrast agents. Also, as rapid changes in tumor vascularity and permeability were expected, it was important to assess the two contrast agents during the same imaging session. Since our primary aim was the follow up using ferumoxytol perfusion and to compare CBV changes between treatment groups, ferumoxytol was injected first for perfusion assessment. Evaluating changes in contrast enhancement using gadodiamide was our secondary aim, it was applied 10 to 15 minutes after ferumoxytol.

Rats were imaged before and 24, 48, and 72 h after treatment with the antiangiogenic agent bevacizumab or the corticosteroid dexamethasone.

5.2.5.2 Image processing

Data was sent to a central server and images were downloaded to a PC, where the postprocessing took place. T-I curves were studied individually. From the PWI data, CBV maps were created using Lupe (Lund, Sweden) perfusion software. rCBV values were calculated on an ROI basis as a ratio of the tumor blood volume to a normal appearing (contralateral) brain tissue. Using the information from the serial T1w DCE scans, the vessel permeability was evaluated by determining the time-to-peak (TTP) enhancement (63) in the same tumor ROI used for perfusion measurement. ROI-based analysis was performed using MIPAV software (Medical Image Processing, Analysis and Visualisation; http://mipav.cit.nih.gov).

5.2.6 Statistical analysis

Changes in rCBV and TTP enhancement were statistically analyzed throughout the study using repeated measurements of two-way analysis of variance with Tukey's post hoc statistical test. rCBV and TTP enhancement are displayed as means±s.e.m. $P < 0.05$ was considered significant.

6 RESULTS

6.1 Clinical studies

Twelve patients were enrolled (age range, 32–65 yr; mean age, 51.2 yr; nine men; three women) with either primary malignant (n =11) or metastatic (n=1) brain tumors (Table 2). All patients provided written informed consent and all completed the administration of GBCA and ferumoxytol. There were no adverse events attributed to either agent. All but one patient completed the delayed magnetic resonance series at both field strengths. One patient did not tolerate the complete series of scans and only completed the series through the 24- to 28-hour scan. Five patients had surgery between 24 and 48 hours after ferumoxytol administration.

Table 2. Patient characteristics and qualitative assessment of ferumoxytol vs. gadodiamide enhancement

#	Diagnosis	Age	Prior Therapy*	Regional correlation	Enhancement characteristics	Enhancement intensity**
1	**GBM**	61	C,R	Yes	FE more peripheral, growing over time	G
2	**GBM**	39	C,R	Yes	FE more peripheral, growing over time	G
3	**GBM**	65	-	Yes	FE more peripheral, growing over time	=
4	**High grade glioma**	48	-	Yes	FE more peripheral, growing over time	=
5	**Oligodendroglioma**	41	C	Yes	FE more peripheral, growing over time	G
6	**Oligodendroglioma**	63	-	Yes	Less spots visible with FE	GG
7	**Breast carcinoma metastasis**	55	C,R	Yes	FE growing over time	=
8	**GBM**	58	C,R	Yes	FE more peripheral, growing over time	G
9	**Oligodendroglioma**	61	C	Yes	FE enhancement much smaller	G
10	**Malignant pineal tumor**	32	C,R	No	Multiloculated cysts	=
11	**High grade glioma**	59	C,R	Yes	Faint FE enhancement	GG
12	**GBM**	32	C	Yes	FE growing over time	F

* C: chemotherapy, R: radiation

** "G/GG": gadodiamide more/much more intense; "=": about the same intensity; "F": ferumoxytol more intense

Table 2

6.1.1 Ferumoxytol enhancement time course

In postcontrast MRI scans, there was no major difference between the two field strengths, although 1.5T provided somewhat better contrast. RF coil inhomogeneities were not as pronounced as they were at 3T (Figure 4). At 1.5T, the curves reached their highest intensity at either 16 to 20 hours (n=3) or at 24 to 28 hours (n=9). At 3T, the individual curves were similar to those at 1.5T, but the peaks were somewhat more scattered, with two peaks at 4 to 6 hours, three at 16 to 20 hours, six at 24 to 28 hours, and one at 48 to 52 hours. Evaluating the averaged curves, we found that SI rises almost to peak intensity at 16 to 20 hours after ferumoxytol injection, peaks at 24 to 28 hours, and then begins to fall; however, contrast enhancement is still evident after 72 hours (Figure 5). The area of ferumoxytol enhancement expanded gradually with time, but never exceeded the area of increased signal on T2w slices (Figure 6). In seven patients, the intensity of gadodiamide enhancement was greater than of ferumoxytol; in one patient, ferumoxytol enhancement was greater; and in the remaining four patients, the intensity was similar (Table 2). The lesions were clearly detectable at 0.15-T in all five patients who underwent intraoperative MRI scanning (Figure 7).

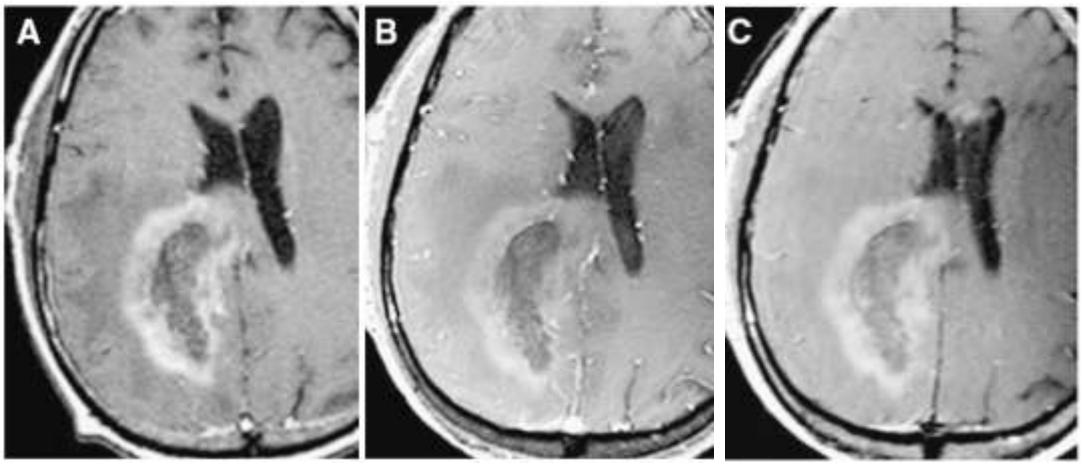

Figure 4

T1w MRI scans showing enhancement 50 hours after ferumoxytol injection on 1.5T fast spin echo (FSE) (A), 3T FFE (B), and 3T TSE (C) sequences. The best contrast was obtained at 1.5T. At 3T, the TSE sequences showed better enhancement than FFE.

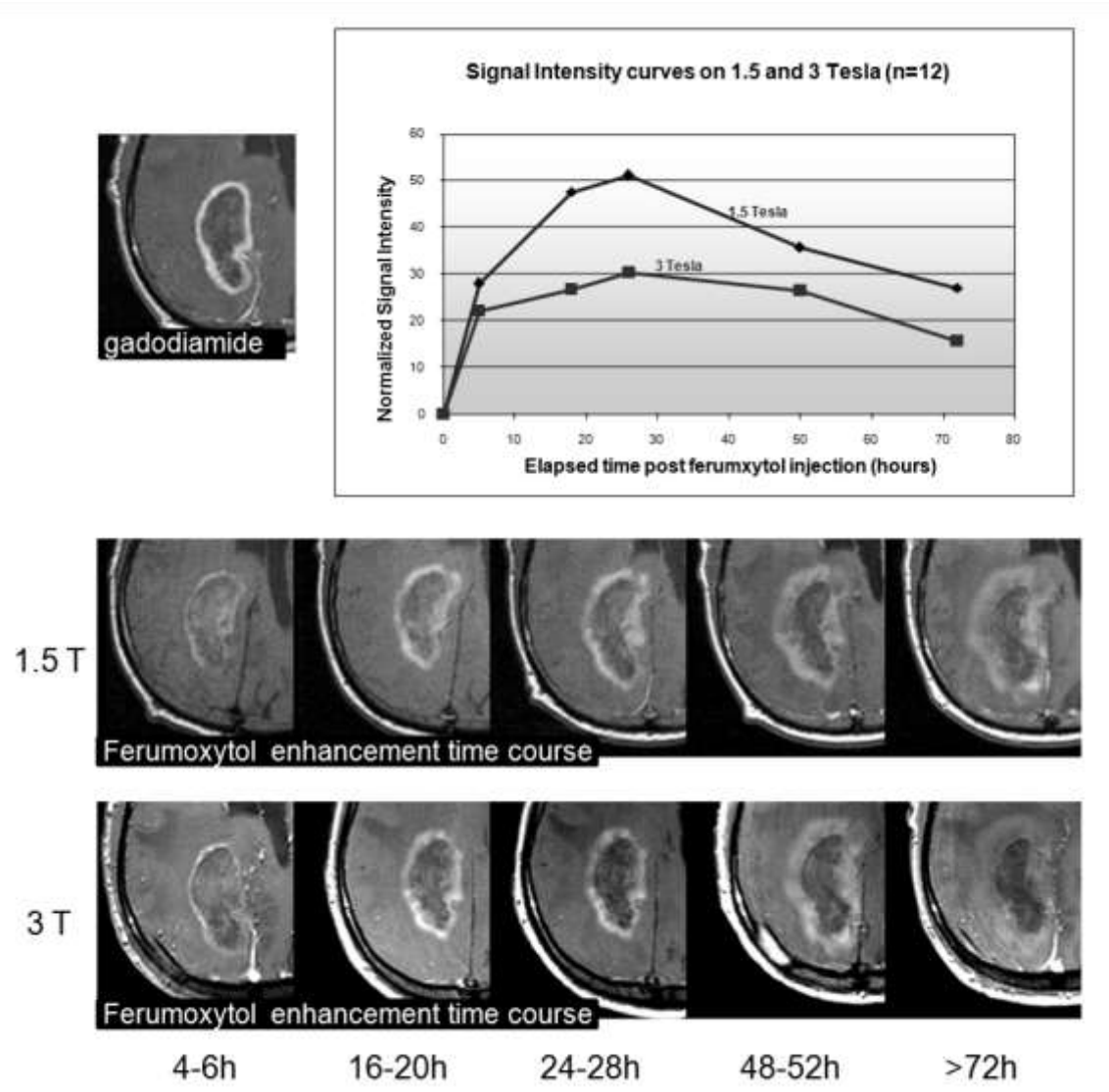

Figure 5

Ferumoxytol enhancement time course on 1.5 and 3T. The average intensity peaks at the 24-28 hour time point, which is much longer than with gadodiamide (not shown), which provides the maximum enhancement intensity at 3.5 to 25 minutes after injection.

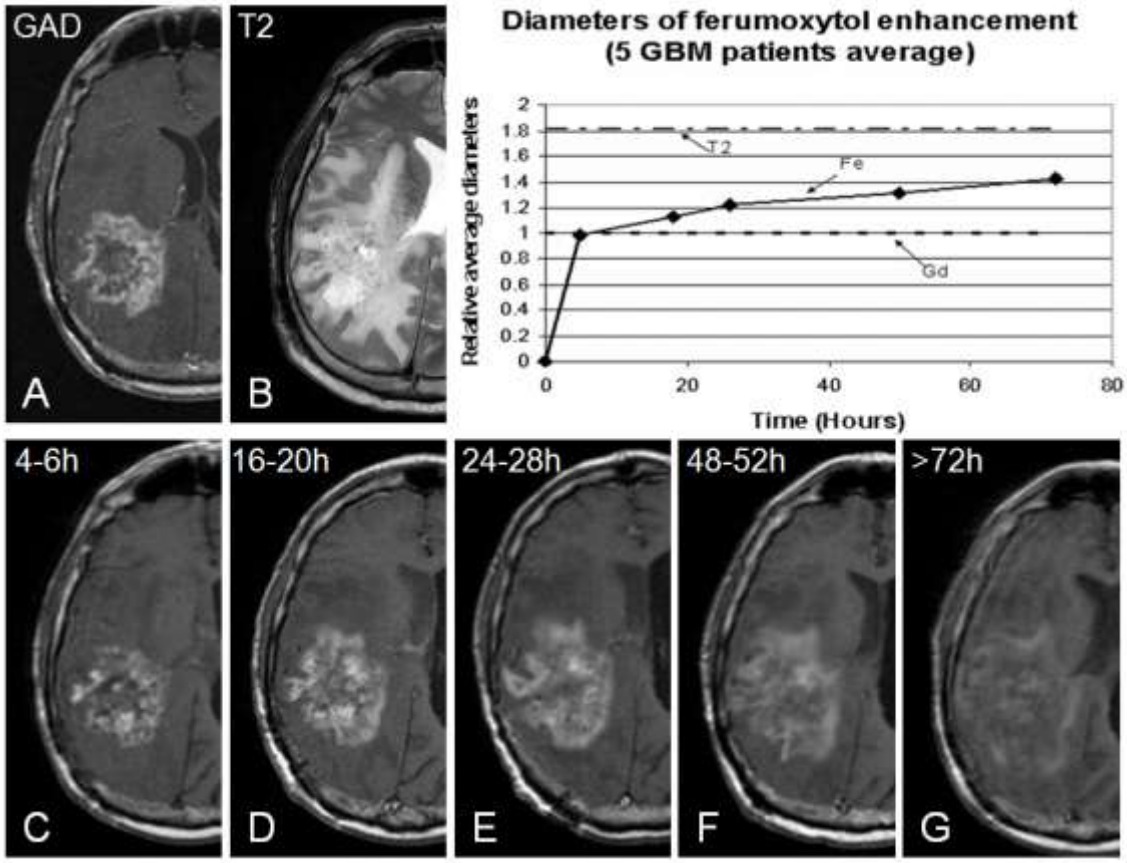

Figure 6

Increase of enhancing area over time following IV ferumoxytol injection. Line graph showing the extent of ferumoxytol enhancement in a GBM patient. The average diameter changes of ferumoxytol enhancement over time (solid line) are compared with the diameter of GBCA enhancement (dashed) and T2w signal abnormalities (dashed dotted). GBCA T1w (A), T2w (B), and post ferumoxytol T1w (C–G) MRI scans at five time points.

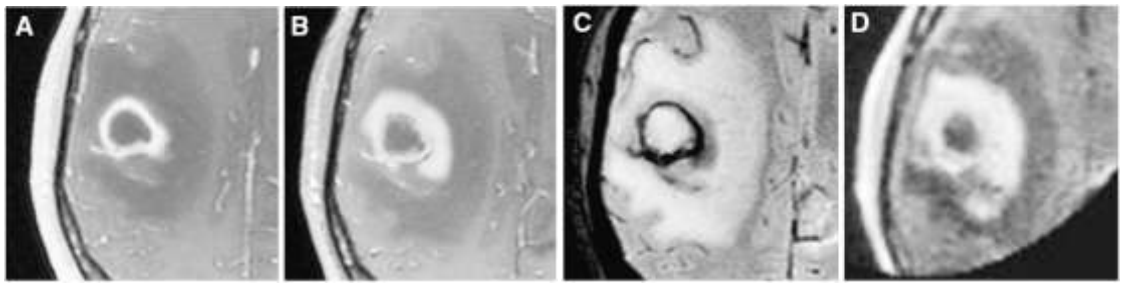

Figure 7

T1w MRI scan showing enhancement with GBCA (A). T1w image (B) and T2w (C) images 24 hours after ferumoxytol infusion. Intraoperative T1w 0.15-T MRI scan 26 hours after ferumoxytol injection (D).

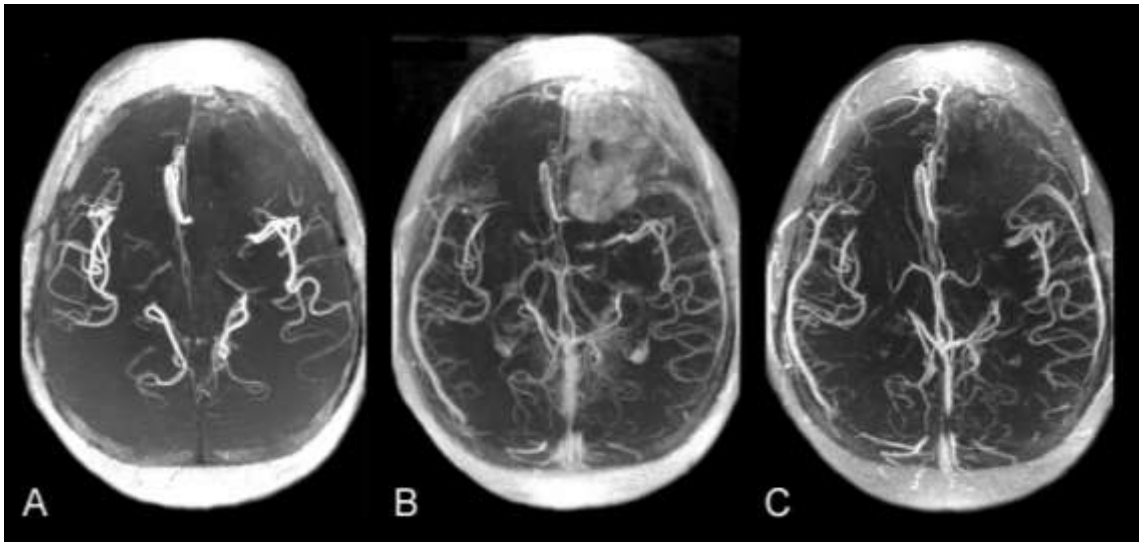

Figure 8

Patient 12. Maximal intensity projection images of TOF MRA without contrast (A). 15 minutes after IV GBCA (B) showing more vascular structures. There is also enhancement in the left frontal tumor. TOF MRA 15 minutes after ferumoxytol infusion (C). More vessels are visible, but there is no enhancement of the tumor.

6.1.2 TOF MRA

Contrast enhanced TOF angiography showed more vascular structures in the brain and within the tumor than without contrast agent. (Figure 8) Because ferumoxytol persists in the vasculature, its beneficial effect may be evident hours after injection. In our studies, both contrast agents allowed visualization of smaller blood vessels in five out of six patients. However, gadodiamide leaked out of the vasculature into the tumor quickly, "contaminating" the TOF images with tumor enhancement. This artifact was seen in four out of six patients.

6.1.3 Quantitative T1 measurement

To assess regional contrast agent uptake, T1-weighted measurements were performed before and after contrast agent administration at 3-T in four study participants, with postcontrast measurements in one additional patient (Figure 9). R1 (R = 1/T1), which is directly proportional to tissue contrast agent concentrations, showed a significant increase in the enhancing lesion after gadodiamide administration (P = 0.026). When R1 values were normalized using areas of normal white matter, the ratio was significantly increased with gadodiamide when compared with precontrast administration or with ferumoxytol administration (P = 0.02).

6.1.4 DSC perfusion imaging

For perfusion imaging, ferumoxytol and gadodiamide rCBV and rMTT parametric maps were comparable for all patients except those with technical difficulties (n = 2). The calculated rCBV and rMTT averages are shown in (

Figure **10**). The enhancing tumor showed significantly higher rCBV than the peritumoral area with both GBCA (P = 0.0009) and ferumoxytol (P = 0.0007). In comparing the rMTT values of the same ROIs, there was no significant difference (GBCA, P = 0.54; ferumoxytol, P = 0.42). When comparing gadodiamide and ferumoxytol, there were no statistically significant differences between the averages of rCBV or rMTT values in enhancing tumor or peritumoral areas (tumor rCBV, P = 0.42; tumor rMTT, P = 0.67; peritumoral rCBV, P = 0.13; peritumoral rMTT, P = 0.11). The perfusion T-I curves (Figure 11) showed a remarkable difference between the two contrast agents in three patients. As the contrast bolus entered the brain vasculature, the

local T2w signal rapidly decreased. As the contrast bolus flowed out, the local SI began to increase. At this point, the T-I curve recovers more gradually because of vascular leak with GBCA than with ferumoxytol. Unlike GBCA, the ferumoxytol perfusion curve recovered rapidly to equilibrium.

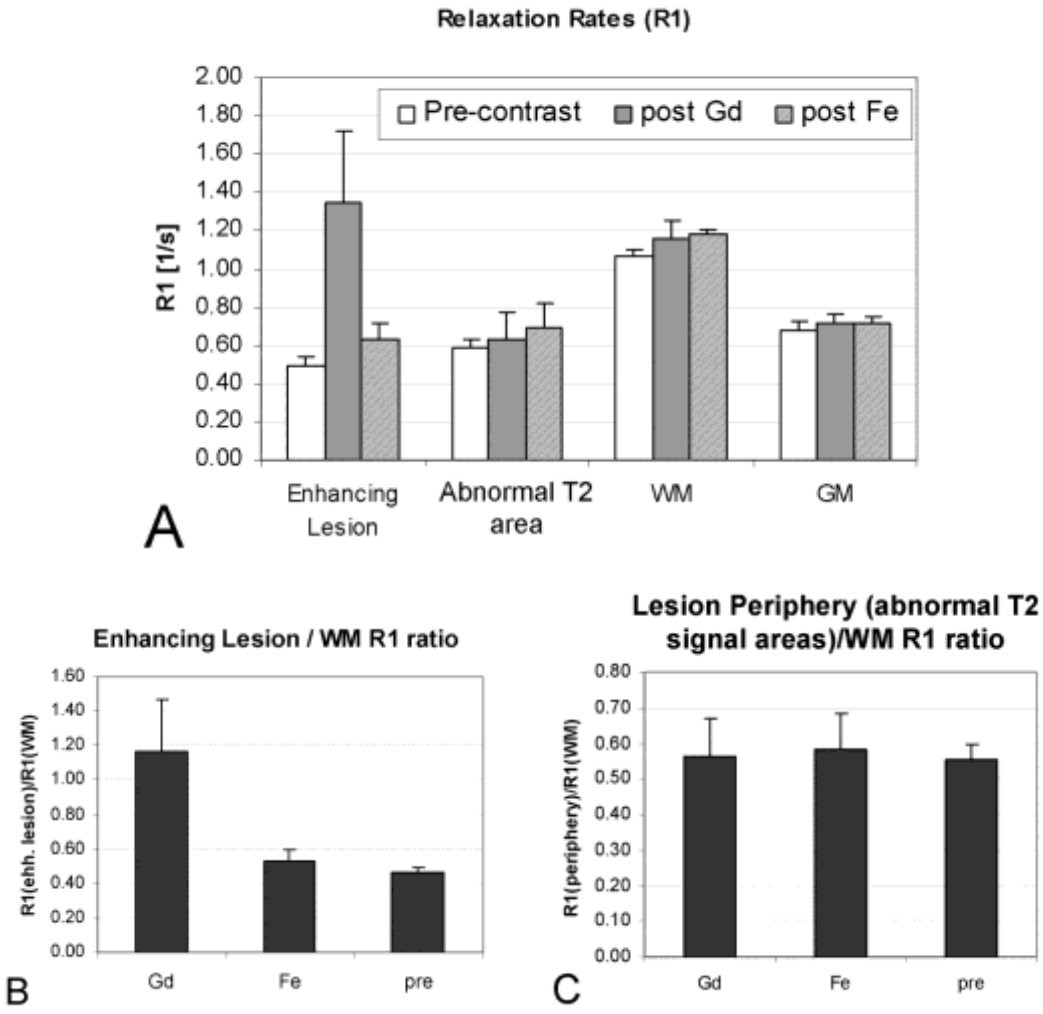

Figure 9

Bar graphs showing the average R1 measurements at 3-T in five patients. (A) comparison of R1 in the enhancing lesion, area of T2- weighted MRI scan abnormality, and normal white matter (WM) and gray matter (GM). (B) normalized comparison of precontrast (pre), gadolinium (Gd) containing contrast agent, and ferumoxytol (Fe) in the enhancing (enh) lesion. (C) comparison of R1 in the areas with abnormal T2 signal.

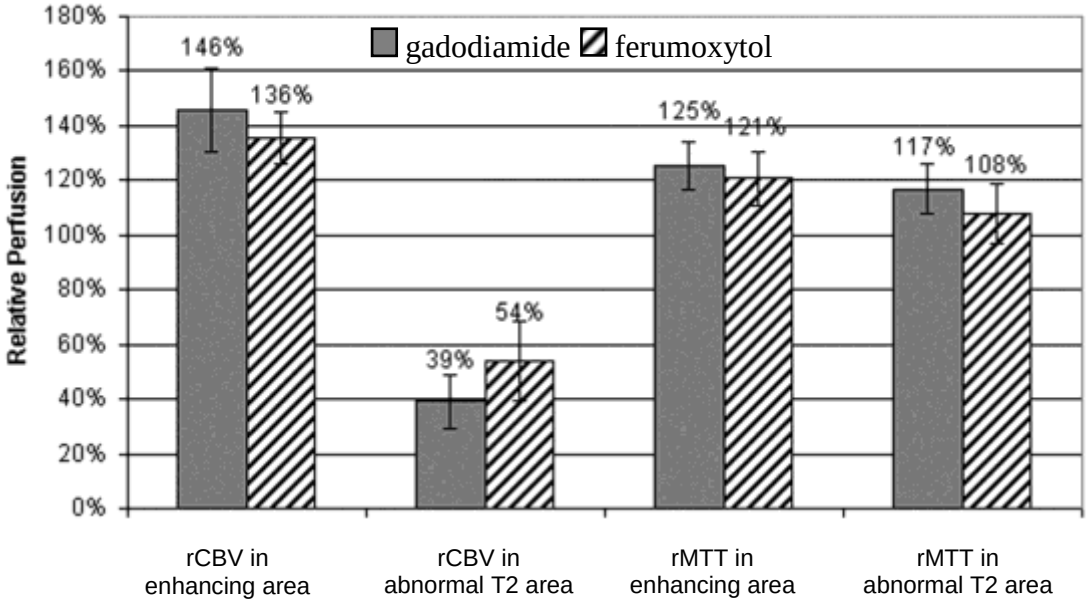

Figure 10

Quantitative assessment of MRI perfusion using gadodiamide vs. ferumoxytol. rCBV (n=10) and rMTT (n=8) were assessed using ROIs of the enhancing tumor and the surrounding high T2w signal area compared with normal appearing white matter.

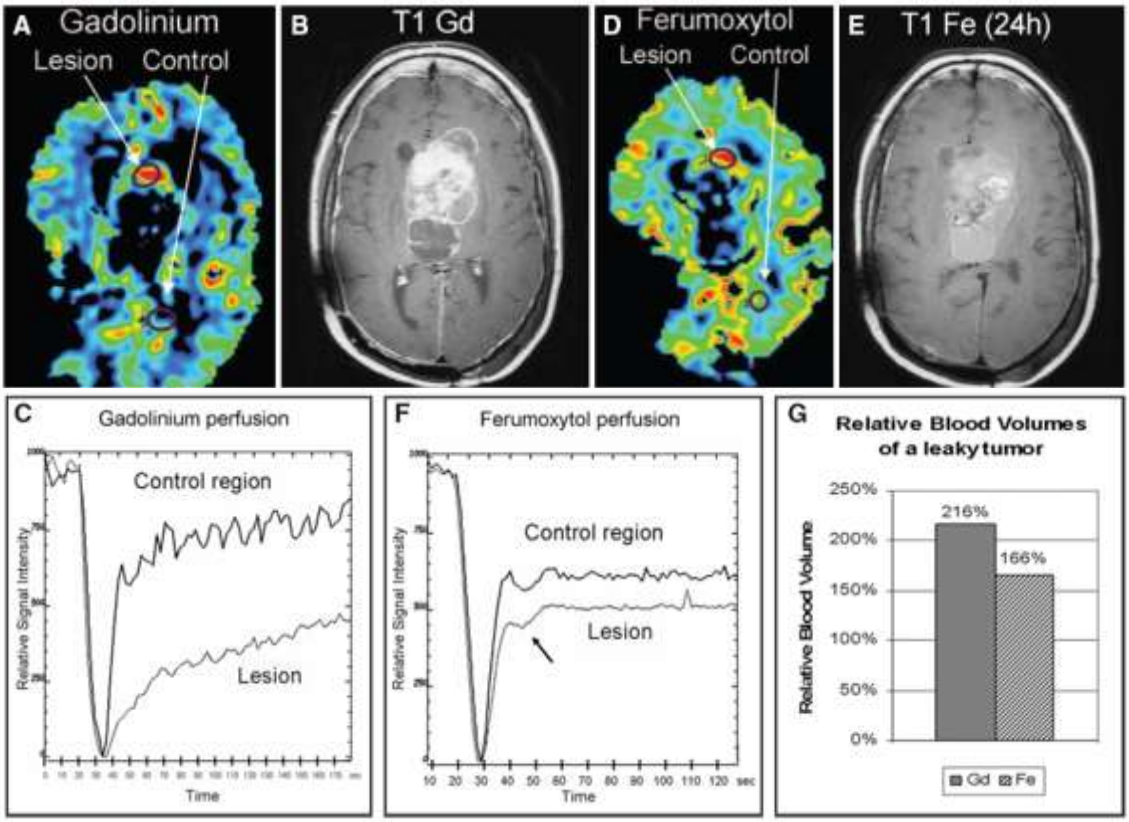

Figure 11

Patient 10. (A) and (D), CBV parametric maps indicating the ROIs of the lesion and control brain. (B) and (E), T1w postcontrast MRI scans. (C) T-I curves with gadodiamide; the decreased slope of the recovery curve indicates GBCA leakage in the tumor region. (F) with the infusion of ferumoxytol, the lesion shows a curve similar to the control region; no leakage is seen (arrow indicates the recirculation). (G) bar graph showing relative blood volume values.

6.2 Preclinical studies

6.2.1 Tumor model

Half of the animals developed visible tumor growth 14 to 42 days after stereoscopic intracranial tumor cell inoculation. When tumor volumes reached the 50 mm^3, animals could be scheduled for 12T dynamic MR scanning. High resolution T2w scans depicted the tumors well, and could be used to plan the DSC and DCE imaging to ensure a precise placement of slices throughout the longitudinal experiment. (Figure 12) MR imaging showed a good correlation with histology (Figure 13).

Figure 12

High resolugion T2w scans of a rat brain in coronal (left) and axial (right) planes at 12T. Tumor growth is clearly visible 4 weeks after intracerebral injection of U87MG cells (arrows).

Figure 13

Comparison of MRI and Histology in U87 glioma xenographed model. (A) T2w MR image delineates the hyperintense mass. (B) Hematoxylin-stained histological section shows matched tumor volume. (C) On the Perl's iron-stained section, there is only a minimal ferumoxytol uptake in the tumor tissue, with most iron staining found at the tumor periphery as evidenced by brown staining.

A single dose of gadodiamide showed strong enhancement in the tumor, while using ferumoxytol, (even in higher doses) there was no visible (positive or negative) signal change after the first pass. (Figure 14)

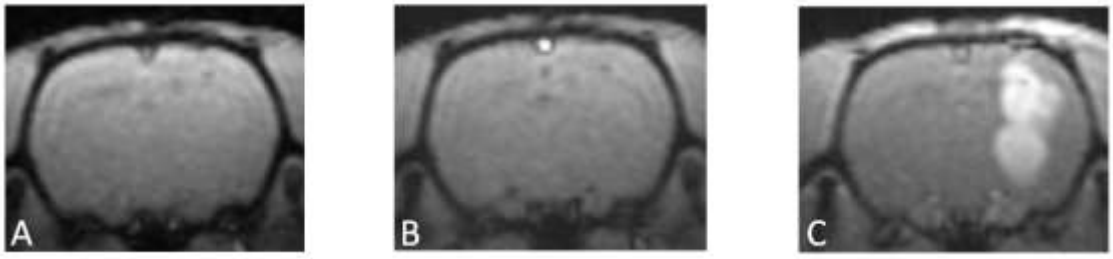

Figure 14

Comparison of ferumoxytol and gadodiamide enhancement in the rat U87 glioma xenographed model. Images on 12T. (A) T1w coronal MR of the rat brain before contrast agent administration. (B) at 60s after administration of IV ferumoxytol (6mg/kg), no enhancement is visible. (C) at 60s post injection of gadodiamide (0.05mmol/kg, IV), the tumor shows increased signal. The small molecular-weight agent can leak rapidly into the U87 tumor parenchyma causing contrast enhancement, but ferumoxytol, at early time points, is effectively a blood pool agent.

6.2.2 MR perfusion using gadodiamide vs. ferumoxytol:

Figure 15 shows a T-I-curve of a brain perfusion study of the normal rat brain on 12T. During MR perfusion measurement the same brain regions are scanned repeatedly, which allows tracking intensity changes caused by a rapid contrast agent bolus. Due to magnetic susceptibility (T2* effect) the T-I curve shows a sudden signal drop when the bolus arrives. As the contrast bolus leaves the tissue, the signal recovers and finally the SI stays constant. (Note the second negative peak, representing recirculation). CBV is usually calculated as the area under the curve. Reliable CBV estimation however assumes that contrast media stays intravascular, which is often not the case in malignant gliomas.

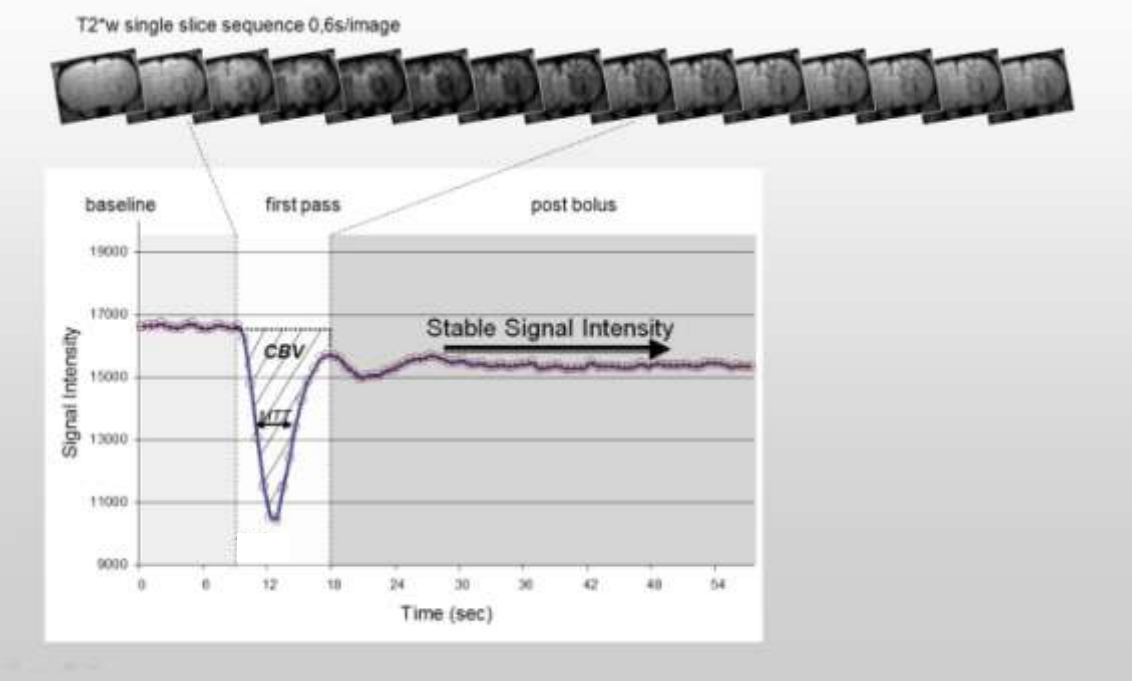

Figure 15

MR Perfusion measurement, T-I curve using USPIO. DSC imaging takes advantage of transient changes in the local magnetic field of the surrounding tissue induced by a bolus of paramagnetic or superparamagnetic tracer passing through the capillary network of an organ. These changes in the local magnetic field can be measured as a signal drop in MRI. CBV is calculated as “area under the curve”.

Testing the model, Intracerebral U87 xenografts appeared to be highly permeable to gadodiamide, but not to ferumoxytol (Figure 14). Owing to the high permeability of gadodiamide, the T2*-based DSC CBV measurement was remarkably affected by contrast agent leakage, as indicated by the rising slope of the plateau following GBCAs (Figure 16). No leakage was detected at these early time points when the blood pool agent, ferumoxytol, was used (Figure 17). The SI post bolus differs between Figure 16 and Figure 17 because the mainly parenchymal GBCAs have storng T1 shortening effects, whereas the intravascular iron oxide nanoparticles have a dominant T2* shortening.

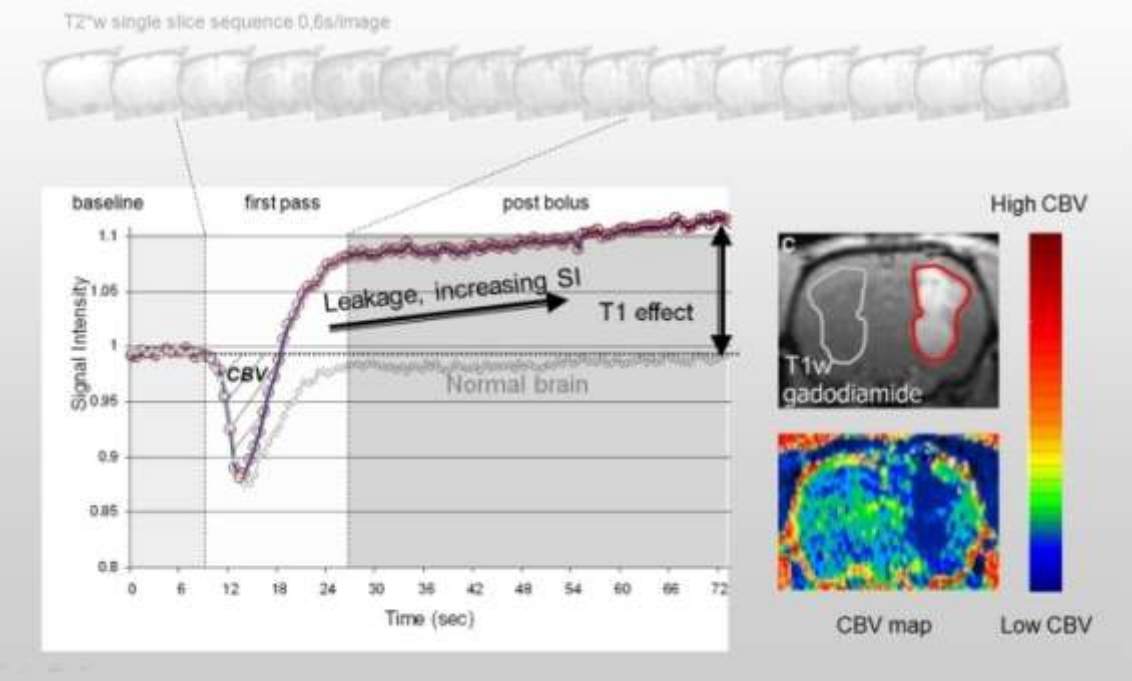

Figure 16

DSC Perfusion in a U87 intracerebral tumor with high vascular permeability for gadodiamide**.** Contrast agent extravasation and T1 effect can cause CBV misinterpretation, in this case underestimation. When a gadodiamide bolus is injected, the rapid contrast agent extravasation will modify even the first pass curve by increasing the SI above the baseline due to T1 shortening effect of the contrast media. Also, in the „post bolus“ phase the SI keeps further increasing. The calculated CBV map shows a decreased CBV value in this known highly vascular tumor, which is obviously an artifact.

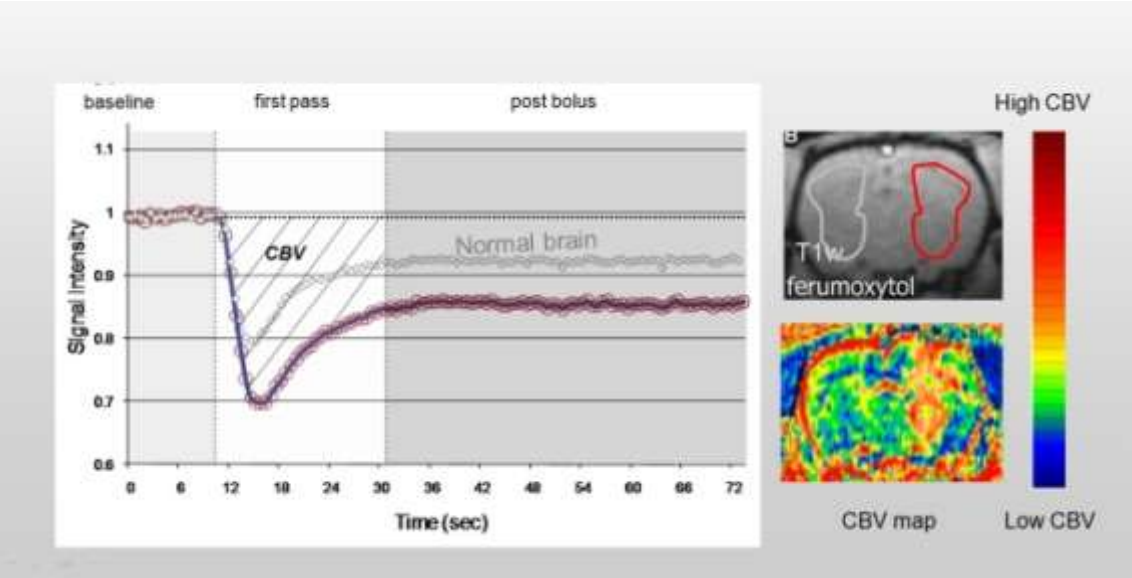

Figure 17

DSC Perfusion in a U87 intracerebral tumor using ferumoxytol. Using ferumoxytol for DSC imaging, no extravasation of the contrast media was seen. rCBV calculation is not compromised by contrast agent leakage. CBV map shows an obvious increase in the tumor.

6.2.3 CBV changes using ferumoxytol in treated animals

Figure 18 shows a non treated animal with increasing tumor size. Blood volume maps show an increasing blood volume value. Figure 19 shows a bevacizumab treated animal with slightly increasing tumor size but decreasing CBV in the tumor.

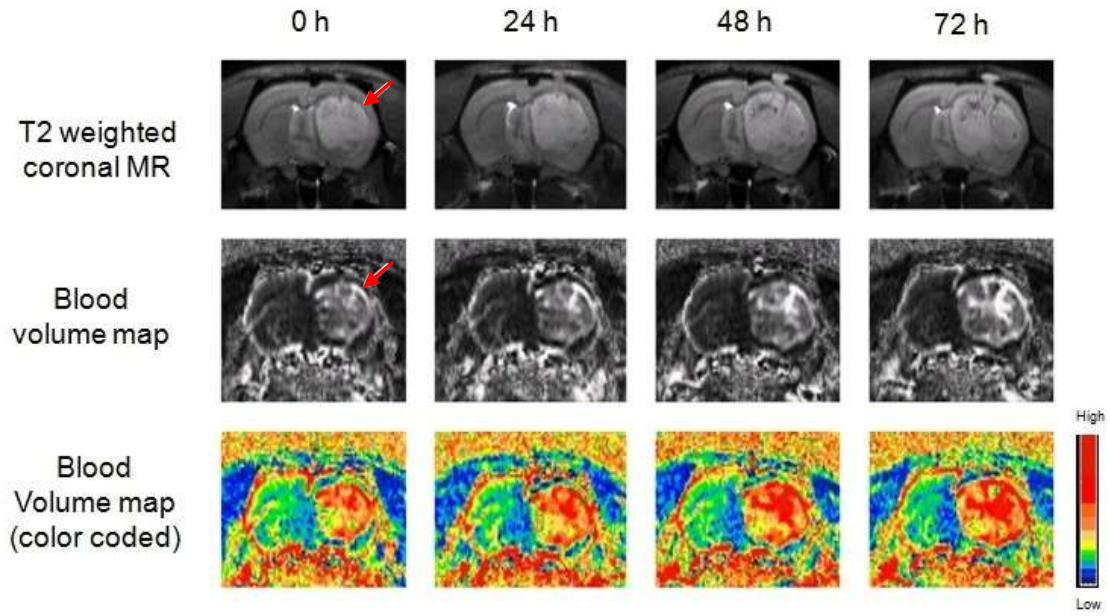

Figure 18

Serial MR imaging of non-treated, control rat. Coronal slices of the brain. The tumor (red arrows) shows an increasing volume with an increasing rCBV measured using ferumoxytol bolus.

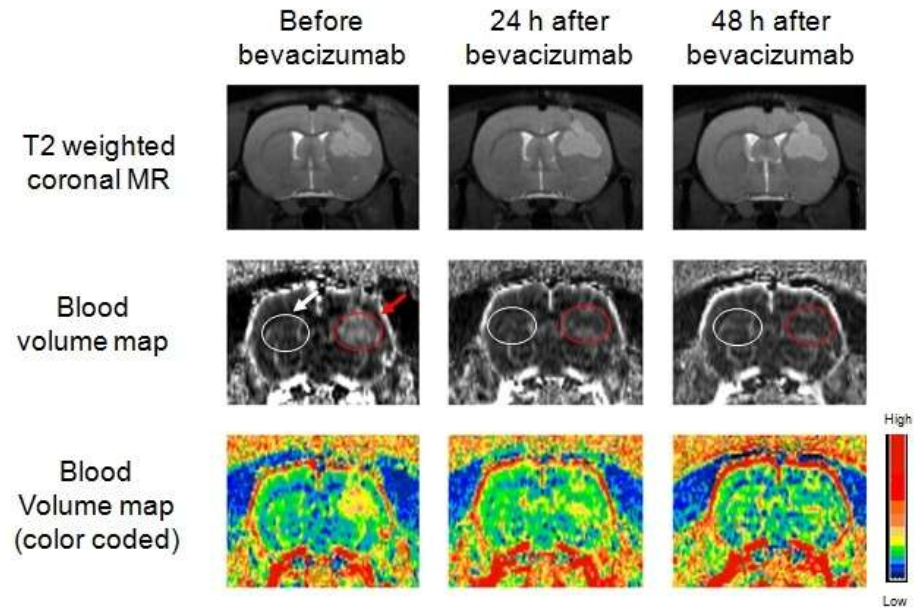

Figure 19

Bevacizumab treated animal. Coronal slices of the brain. As early as 24h post bevacizumab treatment (45mg/kg), rCBV has decreased in the tumor as the parametric

maps indicate. ROIs were defined in the tumor (red arrow) and in the contralateral normal appearing brain (white arrow) to calculate rCBV.

rCBV was found to decrease in the three treatment groups, namely BEV, DEX 2, and DEX 12, but not in the CTR group (Figure 20A). In the BEV group, the initial rCBV (1.628±0.091) decreased significantly in all 24, 48, and 72 h time points to 1.214±0.061, 1.082±0.064, and 1.084±0.052, respectively. In the DEX 2 group, the initial rCBV of 2.130±0.180 showed significant decrease in the 48 and 72 h time points (1.755±0.040 and 1.725±0.098, respectively). In the DEX 12 group, the initial 1.800±0.072 rCBV value decreased significantly at all time points, to 1.380±0.029 at 24 h, 1.286±0.028 at 48 h, and 1.272±0.041 at 72 h. In the CTR group, there was no significant change found from the initial 1.927±0.363 rCBV value. The normalized rCBV in BEV and DEX 12 groups appeared to be significantly decreased compared with the CTR and DEX 2 groups in all the three posttreatment time points (Figure 20B). The difference between the BEV and DEX 12 groups was not significant. The DEX 2 group became significantly different from the CTR group at the 48 and 72 h time points.

6.2.4 Gadodiamide permeability changes

Figure 21 and Figure 22 describe the calculation of TTP. In the BEV group, the initial TTP of 60±19 s increased significantly in all 24, 48, and 72 h posttreatment time points to 125±42 s, 176±50 s, and 194±58 s, respectively Figure 20C). Similarly, in the DEX 12 group, the initial 62±14 secs increased to 107±27 s, 127±41 s, and 133±44 s, respectively. The baseline TTP of 72±17 s in the DEX 2 group and the 58±12 s in the control group has not shown significant changes throughout the study. After normalizing the TTP data to the pretreatment value in each treatment group, there was no significant difference between the groups 24 h after the start of treatment (Figure 20D). At the 48 h time point in the BEV treatment group, the TTP increased significantly to 3.023±0.58 compared with the CTR (1.071±0.05) and also compared with the DEX 2 TTP (1.517±0.25), but it was not significantly different from DEX 12 (1.907±0.16, P = 0.051). At 72 h post-treatment time point, the normalized TTP in the BEV group increased to 3.313±0.59, and was found to be significantly higher than that

in all the three other groups (CTR: 1.110±0.06, DEX 2: 1.581±0.37, and DEX 12: 2.064±0.34). There were no other significant differences between groups.

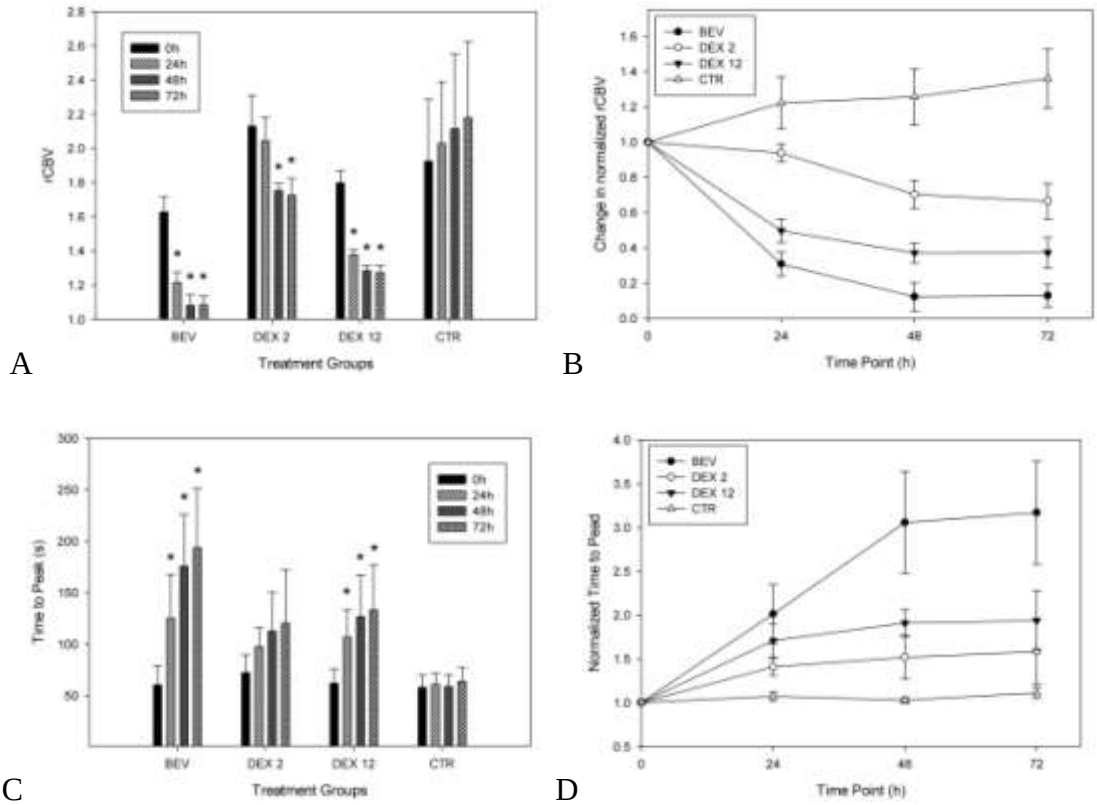

Figure 20

Results of dual agent dynamic imaging throughout therapy in four treatment groups. Dexamethasone and bevacizumab reduce rCBV (measured using ferumoxytol) and increase time-to-peak enhancement using gadodiamide. (A) Relative cerebral blood volume decreases in BEV, and DEX 12 and DEX 2 groups, *Significant changes to pretreatment value (0 h). (B) Normalized rCBV for comparison between treatment groups. Bevacizumab and DEX 12 groups show significant rCBV decrease compared with DEX 2 and CTR groups. (C) TTP increases in BEV, DEX 2, and DEX 12 groups, *Significant changes to pretreatment values (0 h). (D) Normalized TTP for comparison between treatment groups. Bevacizumab treatment shows significant increase in the 48h time point compared with CTR and DEX 2 groups and 72 h post treatment compared with all other groups. Treatment groups BEV: bevacizumab (45 mg/kg) n=5; DEX 2: dexamethasone (2 mg/kg per day) n=4, DEX 12: dexamethasone (12 mg/kg per day) n=5; and CTR: control n=3. (error bars indicate standard error)

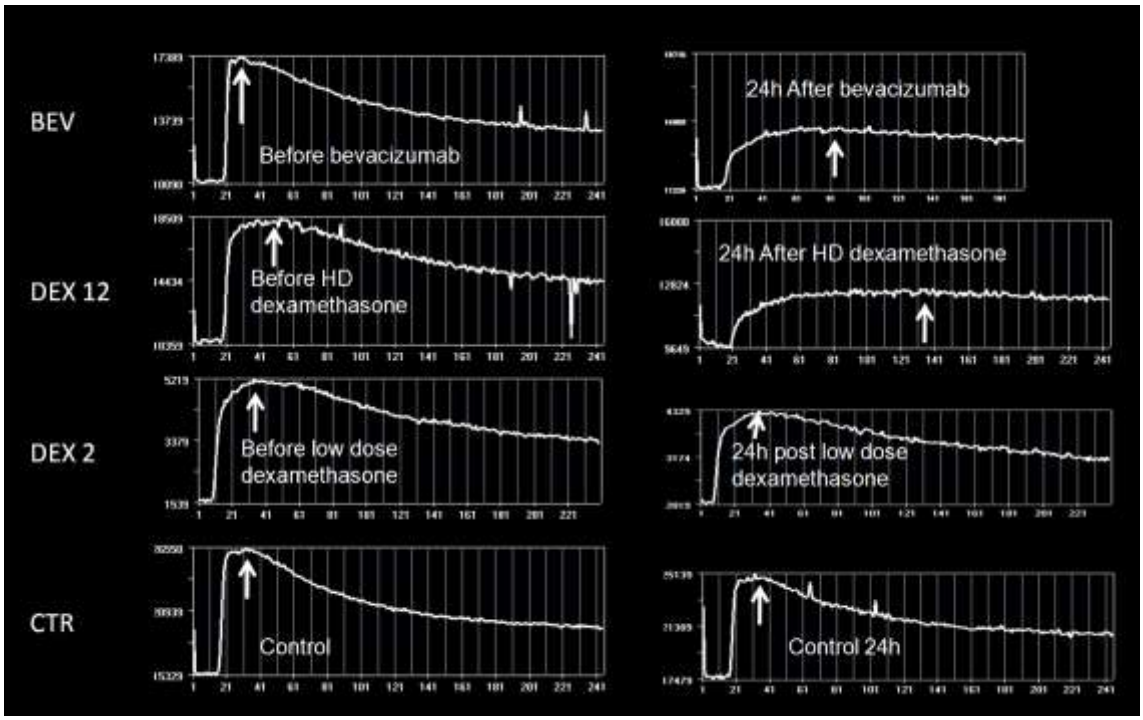

Figure 21

Time-Intensity (T-I) curves of T1w dynamic MRI scans. (x axis: time in sec, y axis: arbitrary intensity unit) One animal in each treatment group before and 24h after treatment. Graphs show signal intensities of the ROI placed in the region of the enhancing tumor. Arrows indicate the maximum enhancement intensity. (note the "spikes" representing acquisition errors, these however don't influence the data substantially)

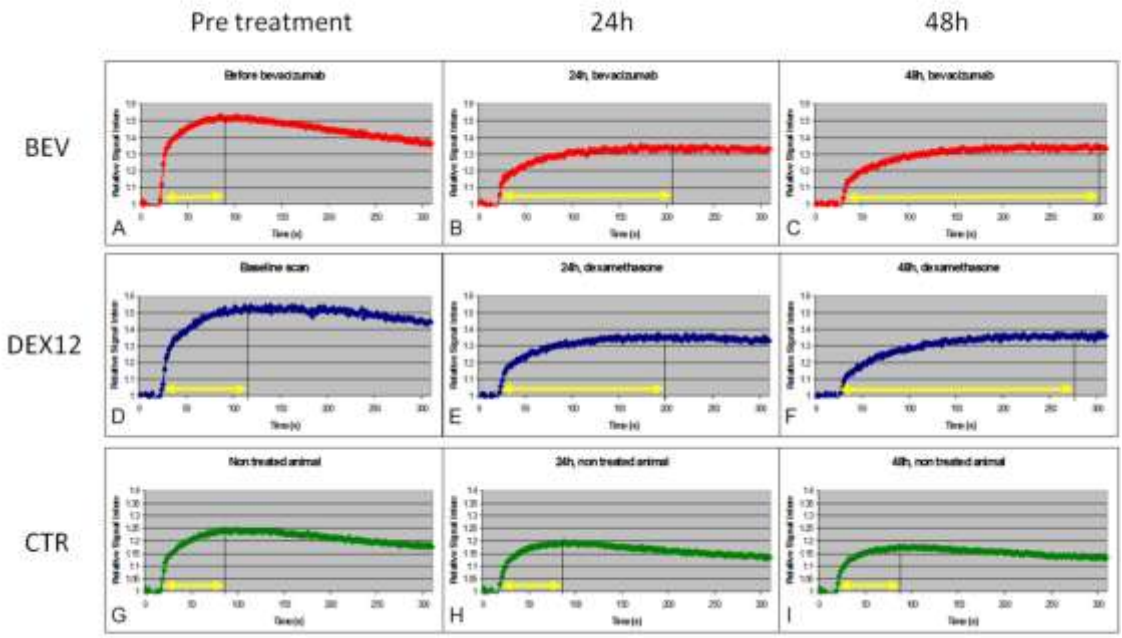

Figure 22

Normalized T-I curves, indicating the TTP enhancement estimation. (averaged curves of multiple animals from each treatment group). Note that the enhancement intensity shows a slight decrease in the control group as well, this might be due to the small amount of USPIO accumulation in the tumor. However, the TTP enhancement does not change significantly (see later).

7 DISCUSSION

7.1 clinical studies

7.1.1 Delayed ferumoxytol enhancement

In this study we performed serial MR imaging in 12 patients with malignant brain tumors. Following intravenous ferumoxytol contrast agent administration patients underwent 1.5 and 3T imaging in 5 time points at each magnetic field until 72 hours. We anticipated a delayed enhancement due to the large particle size and long plasma half life of 14-21 hours. The enhancement intensity showed a peak at approximately 24 hours after administration. This time is subtantially longer than GBCA contrast agents, which show maximum enhancement 3.5 to 25 minutes after IV injection (64). There are three important findings with late ferumoxytol enhancement.

First of all, that the enhancement pattern shows similarity to gadolinium enhancement on T1w images. This assumes a similar mechanism, a leakage through the compromised BBB. This however takes substantially longer, mainly as the particle size is much larger, thus a prolonged plasma half life is also required allowing the slow permeable molecule to reach a substantial extravascular concentration needed to increase signal on T1w scans. The modified carbohydrate coating of the iron compound plays an essential role to grant this property to ferumoxytol, preventing it from rapid intracellular uptake. However in surgical samples, USPIOs were often found intracellular, which assumes iron uptake, and this process might be also important in parenchymal USPIO accumulation (32). Iron oxide nanoparticles are not specific to tumors, enhancement was also found in inflammatory lesions, taken up by reactive cells in the brain (26, 31). Our workgroup has previously reported data with USPIO enhancement in tumors, demyelinating disease, and stroke with ferumoxtran-10 (28, 29). Ferumoxytol may be an indicator of peritumoral macrophages and dendritic cells. In our study, the three patients with GBM who received previous radiation showed less intense enhancement with ferumoxytol than with GBCA. Future studies will investigate the correlation between the effects of therapies and ferumoxytol enhancement. The differences between ferumoxytol and GBCA enhancement may also predict therapeutic efficacy or

demonstrate changes in the permeability of the cerebral and tumor vasculature after treatment, such as radiotherapy. When compared with ferumoxtran-10, ferumoxytol seems to provide somewhat less enhancement. In a previous study, six out of 14 GBMs showed more intense enhancement with ferumoxtran-10 than with GBCA, whereas, in the present study, we only found one case out of five GBMs with slightly more intense enhancement of ferumoxytol than GBCA. This finding is consistent with previous animal studies in which ferumoxtran-10 gave slightly better tumor imaging at the same dose (26). Further randomized investigations are required to prove this finding in humans.

The second important finding is that the enhancement volume is increasing over time, which is very pronounced using ferumoxytol, extending beyond the GBCA enhancing region into the region with pathologic T2 signal. However a somewhat similar phenomenon can be seen with gadodiamide or other GBCA, if images are taken in different time points after injection. This often poses diagnostic problems in follow up MRI studies in which the post gadolinium T1w scans are performed with different delays after injection. A postponed contrast administration can result in a larger enhancing area with somewhat less sharp borders. It is well known that the GBCA-enhancing region for glial tumors is just the "tip of the iceberg" and that tumor cells are distributed well outside of this region (65). The mechanism of the increasing enhancing volume is not fully understood, however a passive diffusion into the non-gadolinum enhancing region of the tumor infiltrated tissue might be one of the mechanisms after the particles crossed the disrupted BBB and entered into the interstitial space. The diffusion should follow the least resistance, and tumor infiltrated area with interstitial edema might favor passive diffusion. On the other hand, areas with very low vascular permeability could show enhancement after a longer period of time, and therefore increasing the enhancing volume. Nevertheless none of the mechanisms of increasing enhancing volume has been proven in this study.

The third important finding is, that unlike GBCA, the higher magnetic field strength seems to decrease the SI on T1w images 24h post ferumoxytol. In T1w scans the lower SI on 3T versus 1.5T units was most likely caused by the strong T2- shortening effect of

ferumoxytol, which is more prominent when using a higher magnetic field. Our ongoing, in this work not detailed studies suggest that using a 7T scanner, ferumoxytol enhancement is even less compared to 3T. This observation can be explained with the magnetic field dependence of relaxivities. The r_1/r_2 ratio shows a substantial decrease of superparamagnetic iron oxides, and just a slight decrease of paramagnetic agents like gadodiamide, when increasing the magnetic field strength. (Figure 2)

7.1.2 TOF MRA and T1 measurement

A true intravascular contrast agent would provide ideal visualization of the small tumor vessels. TOF MRA does not require contrast administration, but the use of an intravascular T1 shortening contrast agent eliminates the saturation effect, and allows visualization of small vessels and tumor vascularity at the submillimeter resolution of 3D TOF acquisition (66). In our studies, both contrast agents allowed visualization of smaller blood vessels in five out of six patients. However, gadodiamide quickly leaked out of the vasculature into the tumor parenchyma, "contaminating" the TOF images with tumor enhancement. The lack of visible leakage suggests that ferumoxytol could be a useful intravascular agent depicting the vascular structures. T1 measurements were also performed, as an increase in the T1 values would sensitively indicate contrast agent leakage. The comparison of T1 values before and 10 to 15 minutes after contrast administration indicated that ferumoxytol did not cause significant enhancement during this early phase after contrast administration in lesions that enhanced with GBCA contrast. At early time points, ferumoxytol remains in the vasculature and avoids "contamination" caused by leakage into the extravascular space. This information is essential in the evaluation of DSC scans, and also may give a possibility to perform steady state blood volume assessment, which has already been successfully performed in preclinical experiments (67).

7.1.3 Dynamic imaging

Perfusion studies showed early vascular leakage in three of these cases performed with GBCA but not with ferumoxytol. GBCA leaks across the defective BBB easily, causing the delayed recovery phase that affects the rCBV and rMTT measurements. In this study rCBV was overestimated with the low molecular weight gadodiamide. This is

however not always the case as a result of contrast agent extravasation. Whether an overestimation or an underestimation of the “area under the T-I curve” occurs, mainly depends on the sequence, the applied contrast agent and magnetic field strength. If the dominant effect is an increasing T1 signal due to the parenchymal tracer, a T-I curve will rapidly recover, and also it can increase above the baseline, causing underestimation of rCBV. This type of error was found in our preclinical experiment. If the sequence is strongly T2* weighted, even a parenchymal contrast agent can cause a delayed recovery, increasing the “area under the curve”, thus overestimating rCBV. Perfusion studies performed with ferumoxytol show a much more consistent rapid recovery phase than those with GBCA. The macromolecular size of ferumoxytol is the likely explanation for this difference; the viral-sized iron nanoparticles are much larger than the Gd chelate and cross defects in the BBB slowly. The early intravascular location of ferumoxytol makes it much less susceptible to errors in measurement of perfusion values than GBCA. PWI and the derived measurements may potentially be useful in determining treatment efficacy by quantifying changes in the tumor tissue perfusion (68). Although there is still limited data available regarding how anti-angiogenic therapies affect GBM (15), an intravascular contrast agent would be helpful in the determination of early tumor response because these drugs may primarily influence the tumor vessel permeability and the perfusion before the tumor shrinks. rCBV could be a more sensitive surrogate for therapy-induced vascular changes, if contrast agent leakage can be avoided. Possible leakage correction methods have been detailed in the introduction, clinically the preloading technique used most commonly. However new evidence suggests that the preload method cannot eliminate the confounding effect of leakage in longitudinal studies evaluating antiangiogenic therapy (47). Our clinical findings, the discrepancies on T-I curves between gadodiamide and ferumoxytol, along with inconsistent rCBV calculation made us design the (in this work detailed) preclinical investigation in which these beneficial properties of ferumoxytol could be exploited.

7.2 Preclinical studies

Based on our pilot clinical study (detailed in this dissertation) ferumoxytol was found to be a suitable T2 relaxation time shortening agent for PWI. My further research with ferumoxytol concentrated on standardized preclinical experiments, allowing a more objective assessment of this iron oxide compound in brain tumor imaging. At this time a new 12T experimental MR system was installed at the Advanced Imaging Research Center at OHSU which made possible to perform DCE and DSC imaging in rats. Ferumoxytol showed potentials of assessing the tumor vasculature without being affected by tumor permeability. This feature seemed to be promising in monitoring therapeutic effects, especially during antiangiogenic therapy in which primarily the vasculature is targeted.

The main objective of this study was to test ferumoxytol for MR perfusion measurements in monitoring antiangiogenic tumor therapy. For this purpose we developed a protocol including an intracranial tumor model in rats. We compared DSC imaging using ferumoxytol vs. gadodiamide. Finally we performed serial dynamic MR imaging at 12T with bolus injection of ferumoxytol for DSC and GBCA for DCE pre and post treatment.

7.2.1 Developing the protocol for dynamic MR imaging at 12T

One of the major tasks in the study was to develop a protocol in which early vascular effects of ferumoxytol could be studied. There were numerous problems to solve, including MR sequences using the 12T ultra high magnet. Part of the adjustments (e.g. matching and tuning the receiver coil) had to be done manually to receive adequate signal. Stabilizing the tray to avoid vibration, and positioning the animal had to be tested for optimal result. Even though the scans were planned short, the technical issues increased the scan time substantially, therefore a heating mechanism had to be installed and the proper temperature had to be set to keep the animals warm. Another main issue was the tumor model, which appeared to be inconsistent, with low number of tumor bearing animals. Shortly before the actual study was started, our workgroup found that cyclophosphamide pretreatment 24h prior to tumor cell inoculation can facilitate tumor growth. Throughout the study animals underwent anesthesia multiple times. The intraperitoneal ketamine – diazepam combination, which was used for tumor

inoculation appeared to be unsafe in our tumor bearing animals, insufficient doses resulted in substantial motion artifacts and overdosing could cause cardio-respiratory insufficiency and death. Medetomidine, combined with a reduced dose of ketamine appeared to be a safe combination resulting in a 1 to 2 hour long motionless deep sedation. Oxygen saturation and heart rate were monitored throughout the time spent in the magnet. After the MRI sessions, medetomidine was reversed using atipamezole, and animals woke up quickly. Also, animals had to be prepared for contrast bolus injection during MR scanning. We ended up choosing the left external jugular vein, in which a catheter was placed prior to the first dynamic MRI session, using microsurgical tools under the microscope. The PE-50 flexible polyethylene tube was used, which we tunneled toward the back of the animal and the end of the catheter could be hidden under the skin after cauterizing the tip of the tube. The catheter could be reopened and used at following time points again. Animals received heparin to prevent clotting of the tube. Animals with jugular catheters were kept in separate cages. Using this protocol, animals were not lost due to technical issues.

In order to perform dynamic MRI, standardization of the injected contrast bolus was crucial for reproducibility, especially in longitudinal experiment. This however posed problems for the following reasons: The infusion pump had to be placed outside of the magnet room, due to the high magnetic field strength, and the distance between the infusion pump and the animal was long, measuring more than 4 meters. Also, relatively small volumes had to be injected (60µl of contrast agent), with a constant flow rate. To ensure precise delivery, the end of the catheter we preloaded with contast agent. The injected volume of 60µl was equivalent to 22 cm of the PE-50 Tube. The dark brown color of ferumoxytol made this measurement simple. The transparent gadodiamide contrast agent was stained with a small amount of Ewans blue for easier differentiation from saline. Proximal and distal from this preloaded contrast agent, the tubes were filled with saline. The mixing of the saline and contrast agent could be prevented by allowing a minimal air bubble in both ends of the contrast bolus in the PE-50 tube.
To provide a consistent flow rate we used an infusion pump. The distance between the pump and the animal was bridged with 3 tubes used for human contrast agent perfusion connected together and filled up with saline and connected at one end to the injector,

and on the other end to the PE-50 tube which was previously filled with contrast agent. This rigid system provided a good coupling between the infusion pump and the animal. The contrast bolus remained short as required. The above detailed system seemed to be consistent and reproducing bolus contrast agent injections did not pose challenges any more. Subsequent and currently ongoing preclinical studies are still using this same method for dynamic MRI studies.

7.2.2 DSC imaging using gadiodiamide vs. ferumoxytol

The comparison of ferumoxytol vs. gadodiamide DSC perfusion measurement in this tumor model was our next objective, since our clinical study showed a discrepancy in rCBV values of highly permeable tumor regions between these two agents. The U87 tumor model appeared to be highly permeable for gadodiamide, and not permeable for ferumoxytol, therefore this model was suitable to test DSC perfusion imaging and the effect of contrast agent leakage. As expected there was a substantial difference between the results. The rapid extravasation of gadodiamide contrast media caused a rapid increase of the SI, which increased above the baseline during the first pass, good visible on T-I curve, thus underestimating the rCBV. Because here the T1 shortening effect was also present of the parenchymal contrast agent, our results were different found in our clinical study using a primarily T2* weighted sequence. When ferumoxytol was applied, the T-I curve did not show signs of extravasation, and the rCBV was found high in the tumor, as expected in a histologically highly vascular tumor.

7.2.3 Dual agent imaging

We tested dual-agent dynamic contrast MRI to assess early vascular changes after antiangiogenic therapy in comparison to corticosteroid treatment. Our purpose was to separate the measurements of vascular permeability and perfusion, thus minimizing the confounding effects that can cause substantial errors and potential misinterpretation of the rCBV results derived from leakage of small molecular weight contrast agent. Therefore ferumoxytol was used for DSC measurement, and gadodiamide for assessing vascular permeability. As rapid changes in tumor vascularity and permeability were expected, it was important to perform these measurements during the same imaging session. First, using a T2*-based technique, the blood pool USPIO agent ferumoxytol provided information about the tumor vasculature. Second, DCE T1w imaging was

performed using GBCAs to monitor BBB leakage. This dual-agent technique could help in the early assessment of treatment response after antiangiogenic drugs, as it allowed independent evaluation of tumor blood volume and vascular permeability in the same imaging session (69). The dual agent imaging method could be successfully applied with only a minimal confounding effect. The only relevant confounding effect was that the arterial input function for the DCE (second) injection could not be obtained due to high concentration intravascular iron oxide particles. Therefore changes is vascular permeability was expressed as changes in TTP enhancement. A minimal iron uptake in the tumor from previous injections and the intravascular ferumoxytol slightly decreased the maximum enhancement intensity, but did not alter the TTP as seen in non treated animals. Substantial iron accumulation was only found in necrotic areas of larger tumors.

7.2.4 Antiangiogenic drugs vs. corticosteroids

Corticosteroids are often used in CNS tumor patients. High-dose bolus therapy can be indicated in emergencies (e.g., spinal shock) to rapidly decrease edema to prevent irreversible tissue damage and regain neurologic functions. It remains unclear whether changes in CBV play an important role in the rapid clinical effects of glucocorticoids (70-72). Our results show analogous effects of dexamethasone and bevacizumab on both GBM permeability and blood volume in the early phase of treatment, although the effects differ in magnitude at the tested doses. Both bevacizumab and the higher-applied dose of dexamethasone (12 mg/kg/day) acted rapidly, decreasing the tumor rCBV and extending TTP enhancement within 24 h. Bevacizumab appeared to be significantly more effective than dexamethasone in the 2 mg/kg per day dose (which is an accepted animal dose, but would be too high for humans). The higher 12 mg/kg per day dose was used to test if increasing the steroid dose could reach the effects of bevacizumab, although this high steroid dose would never be tolerated in humans. The profound effect of bevacizumab, and small molecular weight antiangiogenic drugs, as recently reported (59, 73), on tumor vasculature call into question the use of contrast enhancement alone as an adequate measure of tumor response. It also calls into question whether bevacizumab decreases chemotherapy delivered to brain tumors, as opposed to non-CNS tumors. The increased survival when bevacizumab is used with chemotherapy in

GBM, both preclinically (13) and clinically (18), is likely due to both a ‘steroid-like effect’ and a cytotoxic effect. However, as pointed out by Jahnke et al. in animals and Norden et al. in patients, progression after bevacizumab was often associated with a larger ratio of nonenhancing to enhancing tumor (3, 13). Indeed, rodents given bevacizumab and carboplatin died with larger tumor volumes than control animals, possibly because of the ‘steroid-like effect’ on tumor-associated vasogenic edema of bevacizumab. Our current study analyzed the microvascular changes in early time points after bevacizumab versus dexamethasone treatment. A single high dose of bevacizumab resulted rCBV and TTP changes, which was significant in all posttreatment time points. The mechanism behind this rapid effect is still not fully understood. Further investigations (including long term follow-up and survival analysis) will clarify the usefulness of USPIO perfusion and DCE with GBCAs in monitoring antiangiogenic treatment.

7.2.5 Future directions

Our data implies differences between the current standard contrast agent, gadodiamide, and complementary agents, such as ferumoxytol. This study does not show that ferumoxytol enhancement would define tumors better than GBCA. However, we think that ferumoxytol will assess the CBV perfusion parameter more accurately than GBCA because it does not leak out of blood vessels. The technical lessons learned will allow for future, more rigorous studies designed to examine the role of dynamic MRI scans using iron oxide nanoparticles for the evaluation of brain tumor therapy.

Ferumoxytol is now commercially available. Our workgroup is studying potential applications in evaluating early therapeutic response in patients with high grade gliomas. Ferumoxytol perfusion holds promise in differentiating true tumor progression from pseudoprogression (19).

8 CONCLUSIONS

Ferumoxytol, a bolus injectable USPIO may serve as a complimentary agent to improve localization, characterization, and follow-up in CNS malignancies. Using dynamic contrast MRI studies, it will be invaluable in the future for monitoring therapeutic responses to antiangiogenic chemotherapies. Ferumoxytol, in particular, is an exciting and powerful tool that is FDA approved and can be used to study a variety of CNS pathologies.

We suggest that ferumoxytol-based PWI MRI holds great promise to evaluate tumor behavior, response to therapy, and the effects of different angiogenesis inhibitors in human GBM, with potential use in other brain tumors as well.

New information learned in these studies is the following:

1. Ferumoxytol can be used as an MR contrast agent in CNS malignancies. Enhancement intensity peaks around 24 hours after intravenous administration. In most cases enhancement on T1w scans is somewhat less intense than at GBCA.
2. In early time points ferumoxytol remains intravascular, and the vasculature can be depicted by TOF MRA, without confounding effect of contrast extravasation. The bolus injectable ferumoxytol is suitable for DSC perfusion measurement.
3. Unlike GBCA, ferumoxytol enhancement on T1w scans shows a higher intensity at lower magnetic field strength.
4. Dual agent imaging with ferumoxytol followed by GBCA can be beneficial to evaluate the contrast agent leakage and also the rCBV with minimal confounding effect in the same imaging session.
5. The U87 tumor model is highly permeable for GBCA, but not for ferumoxytol. Using USPIO, the misinterpretation of rCBV derived from contrast agent extravasation can be prevented.
6. Bevacizumab treatment causes a rapid decrease in both tumor rCBV and also blood brain barrier permeability. This effect is similar to a high dose corticosteroid treatment.

9 SUMMARY

9.1 Summary in English

Ferumoxyol, a USPIO MRI contrast agent has been studied in this work for imaging CNS malignancies. In patients, ferumoxytol showed a suitable contrast enhancement 24h post administration on T1w images, comparable to GBCA at clinically relevant magnetic field strengths. Still, due to a somewhat different mechanism of contrast agent accumulation in the extravascular space, enhancement patterns can vary between these two types of contrast agents. MR perfusion measurement using ferumoxytol was also tested, which may be beneficial compared to GBCA, because of its strong T2* relaxation time shortening effect, and also since the nanoparticle stays intravascular early after injection, thus free from leakage, therefore rCBV calculation is not compromised. In light of these results, the second half of this work discusses a preclinical dual agent imaging protocol, in which longitudinal study ferumoxytol perfusion scan was followed by a permeability measurement using GBCA in the same imaging session. U87 glioma tumor bearing animals underwent serial imaging before and after bevacizumab antiangiogenic therapy. A dramatic rCBV and permeability decrease was observed as early as 24h post treatment. These findings were similar, but more pronounced compared to high doses of corticosteroids. This work is a step forward in tumor treatment response assessment using advanced dynamic MR imaging techniques, which may complement the currently used, mainly contrast enhancement based response criteria. These results may help solving diagnostic problems of pseudoresponse and pseudoprogression, which is one of our most relevant future directions.

9.2 Summary in Hungarian

A jelen disszertáció a ferumoxytol, egy vas-oxid tartalmú (ultrasmall superparamagnetic iron oxide, USIPO) MR-kontrasztanyag alkalmazhatóságát vizsgálja rosszindulatú agydaganatokban. Klinikai vizsgálatainkban a ferumoxytol 24 órával az intravénás beadás után mutatott legintenzívebb halmozást T1 súlyozott felvételeken, a klinikumban használt 1.5 és 3 Tesla mágneses térerőkön. A kapott kontraszthalmozás megfelelt a gadolinium-halmozásnál tapasztalt mintázatnak, azonban különbségek is tapasztalhatóak voltak a kissé eltérő halmozási mechanizmusnak megfelelően. A két kontrasztanyag összehasonlítására perfúziós MR-vizsgálatokban is sor került. A ferumoxytol előnyösnek bizonyult ezekben a mérésekben, a kifejezett T2* relaxációsidő-csökkentő hatás miatt, valamint azért, mert ennek nanorészecskéje - méretéből kifolyólag - az érpályában marad, így az rCBV (relative cerebral blood volume) meghatározását nem befolyásolja kontrasztanyag-extravazáció.

Ezen eredmények fényében az itt bemutatott kutatás második fele egy preklinikai kísérletsorozat elvégzése volt, amelyben a ferumoxytol bólussal történő perfúziós mérést követően, gadolinium-beadással következtettünk érpermeabilitásra ugyanazon MR-vizsgálaton belül, kihasználva a két kontrasztanyag eltérő eloszlási és relaxivitásbeli különbségeit. U87 humán gliómákat vizsgáltunk patkányagyban naponta ismételt sorozatos MR-képalkotással bevacizumab, érundonképződés-gátló szer korai vaszkuláris hatásait keresve. 24 órával bevacizumab-injekció után már jelentős rCBV és érpermeabilitás-csökkenés volt észlelhető, hasonlóan, de még kifejezettebben, mint nagydózisú kortikoszeroid adása esetén.

Jelen kutatásunk előrelépést jelent a tumorterápia utánkövetésében dinamikus MR-vizsgálati szekvenciák alkalmazásával, melyek kiegészítésül szolgálhatnak a neuroradiológiában napjainkban használatos, leginkább kontraszthalmozáson alapuló kritériumrendszerhez. Eredményeink segíthetik a jövőben a pseudoresponse és pseudoprogression fontos diagnosztikus problémák megoldását, amely kutatásaink legfőbb távlati célja.

10 REFERENCES

1. Chamberlain, M.C., S.K. Johnston (2010) Salvage therapy with single agent bevacizumab for recurrent glioblastoma. J Neurooncol. 96(2): 259-69.
2. Sorensen, A.G., T.T. Batchelor, W.T. Zhang, P.J. Chen, P. Yeo, M. Wang, D. Jennings, P.Y. Wen, J. Lahdenranta, M. Ancukiewicz, E. di Tomaso, D.G. Duda, R.K. Jain (2009) A "vascular normalization index" as potential mechanistic biomarker to predict survival after a single dose of cediranib in recurrent glioblastoma patients. Cancer Res. 69(13): 5296-300.
3. Norden, A.D., G.S. Young, K. Setayesh, A. Muzikansky, R. Klufas, G.L. Ross, A.S. Ciampa, L.G. Ebbeling, B. Levy, J. Drappatz, S. Kesari, P.Y. Wen (2008) Bevacizumab for recurrent malignant gliomas: efficacy, toxicity, and patterns of recurrence. Neurology. 70(10): 779-87.
4. Brandsma, D., M.J. van den Bent (2009) Pseudoprogression and pseudoresponse in the treatment of gliomas. Curr Opin Neurol. 22(6): 633-8.
5. Cha, S., E.A. Knopp, G. Johnson, S.G. Wetzel, A.W. Litt, D. Zagzag (2002) Intracranial mass lesions: dynamic contrast-enhanced susceptibility-weighted echo-planar perfusion MR imaging. Radiology. 223(1): 11-29.
6. Macdonald, D.R., T.L. Cascino, S.C. Schold, Jr., J.G. Cairncross (1990) Response criteria for phase II studies of supratentorial malignant glioma. J. Clin. Oncol. 8(7): 1277-1280.
7. Law, M., S. Yang, J.S. Babb, E.A. Knopp, J.G. Golfinos, D. Zagzag, G. Johnson (2004) Comparison of cerebral blood volume and vascular permeability from dynamic susceptibility contrast-enhanced perfusion MR imaging with glioma grade. AJNR Am J Neuroradiol. 25(5): 746-55.
8. Stupp, R., W.P. Mason, M.J. van den Bent, M. Weller, B. Fisher, M.J. Taphoorn, K. Belanger, A.A. Brandes, C. Marosi, U. Bogdahn, J. Curschmann, R.C. Janzer, S.K. Ludwin, T. Gorlia, A. Allgeier, D. Lacombe, J.G. Cairncross, E. Eisenhauer, R.O. Mirimanoff (2005) Radiotherapy plus concomitant and adjuvant temozolomide for glioblastoma. N Engl J Med. 352(10): 987-96.

9. Huang, H., J. Held-Feindt, R. Buhl, H.M. Mehdorn, R. Mentlein (2005) Expression of VEGF and its receptors in different brain tumors. Neurol Res. 27(4): 371-7.
10. Reardon, D.A., P.Y. Wen, A. Desjardins, T.T. Batchelor, J.J. Vredenburgh (2008) Glioblastoma multiforme: an emerging paradigm of anti-VEGF therapy. Expert Opin Biol Ther. 8(4): 541-53.
11. Duda, D.G., T.T. Batchelor, C.G. Willett, R.K. Jain (2007) VEGF-targeted cancer therapy strategies: current progress, hurdles and future prospects. Trends Mol Med. 13(6): 223-30.
12. Ignoffo, R.J. (2004) Overview of bevacizumab: a new cancer therapeutic strategy targeting vascular endothelial growth factor. Am J Health Syst Pharm. 61(21 Suppl 5): S21-6.
13. Jahnke, K., L.L. Muldoon, C.G. Varallyay, S.J. Lewin, D.F. Kraemer, E.A. Neuwelt (2009) Bevacizumab and carboplatin increase survival and asymptomatic tumor volume in a glioma model. Neuro Oncol. 11(2): 142-50.
14. Henriksson, R., T. Asklund, H.S. Poulsen (2011) Impact of therapy on quality of life, neurocognitive function and their correlates in glioblastoma multiforme: a review. J Neurooncol. 104(3): 639-46.
15. Pope, W.B., A. Lai, P. Nghiemphu, P. Mischel, T.F. Cloughesy (2006) MRI in patients with high-grade gliomas treated with bevacizumab and chemotherapy. Neurology. 66(8): 1258-60.
16. Hygino da Cruz, L.C., Jr., I. Rodriguez, R.C. Domingues, E.L. Gasparetto, A.G. Sorensen (2011) Pseudoprogression and pseudoresponse: imaging challenges in the assessment of posttreatment glioma. AJNR Am J Neuroradiol. 32(11): 1978-85.
17. Batchelor, T.T., A.G. Sorensen, E. di Tomaso, W.T. Zhang, D.G. Duda, K.S. Cohen, K.R. Kozak, D.P. Cahill, P.J. Chen, M. Zhu, M. Ancukiewicz, M.M. Mrugala, S. Plotkin, J. Drappatz, D.N. Louis, P. Ivy, D.T. Scadden, T. Benner, J.S. Loeffler, P.Y. Wen, R.K. Jain (2007) AZD2171, a pan-VEGF receptor tyrosine kinase inhibitor, normalizes tumor vasculature and alleviates edema in glioblastoma patients. Cancer Cell. 11(1): 83-95.

18. Wong, E.T., S. Brem (2007) Taming glioblastoma: targeting angiogenesis. J Clin Oncol. 25(30): 4705-6.
19. Gahramanov, S., A.M. Raslan, L.L. Muldoon, B.E. Hamilton, W.D. Rooney, C.G. Varallyay, J.M. Njus, M. Haluska, E.A. Neuwelt (2011) Potential for differentiation of pseudoprogression from true tumor progression with dynamic susceptibility-weighted contrast-enhanced magnetic resonance imaging using ferumoxytol vs. gadoteridol: a pilot study. Int J Radiat Oncol Biol Phys. 79(2): 514-23.
20. Faulkner, W.M., (1996) Basic Principles of MRI, http://www.e-radiography.net/mrict/Basic_MR.pdf.
21. Weinstein, J.S., C.G. Varallyay, E. Dosa, S. Gahramanov, B. Hamilton, W.D. Rooney, L.L. Muldoon, E.A. Neuwelt (2010) Superparamagnetic iron oxide nanoparticles: diagnostic magnetic resonance imaging and potential therapeutic applications in neurooncology and central nervous system inflammatory pathologies, a review. J Cereb Blood Flow Metab. 30(1): 15-35.
22. Neuwelt, E.A., B.E. Hamilton, C.G. Varallyay, W.R. Rooney, R.D. Edelman, P.M. Jacobs, S.G. Watnick (2009) Ultrasmall superparamagnetic iron oxides (USPIOs): a future alternative magnetic resonance (MR) contrast agent for patients at risk for nephrogenic systemic fibrosis (NSF)? Kidney Int. 75(5): 465-74.
23. Landry, R., P.M. Jacobs, R. Davis, M. Shenouda, W.K. Bolton (2005) Pharmacokinetic study of ferumoxytol: a new iron replacement therapy in normal subjects and hemodialysis patients. Am J Nephrol. 25(4): 400-10.
24. Weissleder, R., G. Elizondo, J. Wittenberg, A.S. Lee, L. Josephson, T.J. Brady (1990) Ultrasmall superparamagnetic iron oxide: an intravenous contrast agent for assessing lymph nodes with MR imaging. Radiology. 175(2): 494-8.
25. Corot, C., P. Robert, J.M. Idee, M. Port (2006) Recent advances in iron oxide nanocrystal technology for medical imaging. Adv Drug Deliv Rev. 58(14): 1471-504.
26. Muldoon, L.L., M. Sandor, K.E. Pinkston, E.A. Neuwelt (2005) Imaging, distribution, and toxicity of superparamagnetic iron oxide magnetic resonance

nanoparticles in the rat brain and intracerebral tumor. Neurosurgery. 57(4): 785-96; discussion 785-96.

27. Neuwelt, E.A., R. Weissleder, G. Nilaver, R.A. Kroll, S. Roman-Goldstein, J. Szumowski, M.A. Pagel, R.S. Jones, L.G. Remsen, C.I. McCormick, et al. (1994) Delivery of virus-sized iron oxide particles to rodent CNS neurons. Neurosurgery. 34(4): 777-84.

28. Varallyay, P., G. Nesbit, L.L. Muldoon, R.R. Nixon, J. Delashaw, J.I. Cohen, A. Petrillo, D. Rink, E.A. Neuwelt (2002) Comparison of two superparamagnetic viral-sized iron oxide particles ferumoxides and ferumoxtran-10 with a gadolinium chelate in imaging intracranial tumors. AJNR Am J Neuroradiol. 23(4): 510-9.

29. Manninger, S.P., L.L. Muldoon, G. Nesbit, T. Murillo, P.M. Jacobs, E.A. Neuwelt (2005) An exploratory study of ferumoxtran-10 nanoparticles as a blood-brain barrier imaging agent targeting phagocytic cells in CNS inflammatory lesions. AJNR Am J Neuroradiol. 26(9): 2290-300.

30. Neuwelt, E.A., P. Varallyay, A.G. Bago, L.L. Muldoon, G. Nesbit, R. Nixon (2004) Imaging of iron oxide nanoparticles by MR and light microscopy in patients with malignant brain tumours. Neuropathol Appl Neurobiol. 30(5): 456-71.

31. Taschner, C.A., S.G. Wetzel, M. Tolnay, J. Froehlich, A. Merlo, E.W. Radue (2005) Characteristics of ultrasmall superparamagnetic iron oxides in patients with brain tumors. AJR Am J Roentgenol. 185(6): 1477-86.

32. Hunt, M.A., A.G. Bago, E.A. Neuwelt (2005) Single-dose contrast agent for intraoperative MR imaging of intrinsic brain tumors by using ferumoxtran-10. AJNR Am J Neuroradiol. 26(5): 1084-8.

33. Neuwelt, E.A., C.G. Varallyay, S. Manninger, D. Solymosi, M. Haluska, M.A. Hunt, G. Nesbit, A. Stevens, M. Jerosch-Herold, P.M. Jacobs, J.M. Hoffman (2007) The potential of ferumoxytol nanoparticle magnetic resonance imaging, perfusion, and angiography in central nervous system malignancy: a pilot study. Neurosurgery. 60(4): 601-11; discussion 611-2.

34. Chang, K.H., D.G. Ra, M.H. Han, S.H. Cha, H.D. Kim, M.C. Han (1994) Contrast enhancement of brain tumors at different MR field strengths:

comparison of 0.5 T and 2.0 T. AJNR Am J Neuroradiol. 15(8): 1413-9; discussion 1420-3.

35. Rohrer, M., H. Bauer, J. Mintorovitch, M. Requardt, H.J. Weinmann (2005) Comparison of magnetic properties of MRI contrast media solutions at different magnetic field strengths. Invest Radiol. 40(11): 715-24.

36. Krautmacher, C., W.A. Willinek, H.J. Tschampa, M. Born, F. Traber, J. Gieseke, H.J. Textor, H.H. Schild, C.K. Kuhl (2005) Brain tumors: full- and half-dose contrast-enhanced MR imaging at 3.0 T compared with 1.5 T--Initial Experience. Radiology. 237(3): 1014-9.

37. Essig, M., M.A. Weber, H. von Tengg-Kobligk, M.V. Knopp, W.T. Yuh, F.L. Giesel (2006) Contrast-enhanced magnetic resonance imaging of central nervous system tumors: agents, mechanisms, and applications. Top Magn Reson Imaging. 17(2): 89-106.

38. Bjornerud, A., L.O. Johansson, K. Briley-Saebo, H.K. Ahlstrom (2002) Assessment of T1 and T2* effects in vivo and ex vivo using iron oxide nanoparticles in steady state--dependence on blood volume and water exchange. Magn Reson Med. 47(3): 461-71.

39. Ersoy, H., P. Jacobs, C.K. Kent, M.R. Prince (2004) Blood pool MR angiography of aortic stent-graft endoleak. AJR Am J Roentgenol. 182(5): 1181-6.

40. Li, W., S. Tutton, A.T. Vu, L. Pierchala, B.S. Li, J.M. Lewis, P.V. Prasad, R.R. Edelman (2005) First-pass contrast-enhanced magnetic resonance angiography in humans using ferumoxytol, a novel ultrasmall superparamagnetic iron oxide (USPIO)-based blood pool agent. J Magn Reson Imaging. 21(1): 46-52.

41. Schwenk, M.H. (2010) Ferumoxytol: a new intravenous iron preparation for the treatment of iron deficiency anemia in patients with chronic kidney disease. Pharmacotherapy. 30(1): 70-9.

42. Danielson, B.G. (2004) Structure, chemistry, and pharmacokinetics of intravenous iron agents. J Am Soc Nephrol. 15 Suppl 2: S93-8.

43. Ostergaard, L. (2005) Principles of cerebral perfusion imaging by bolus tracking. J Magn Reson Imaging. 22(6): 710-7.

44. Covarrubias, D.J., B.R. Rosen, M.H. Lev (2004) Dynamic magnetic resonance perfusion imaging of brain tumors. Oncologist. 9(5): 528-37.
45. Schaefer, P.W., E.R. Barak, S. Kamalian, L.R. Gharai, L. Schwamm, R.G. Gonzalez, M.H. Lev (2008) Quantitative Assessment of Core/Penumbra Mismatch in Acute Stroke. CT and MR Perfusion Imaging Are Strongly Correlated When Sufficient Brain Volume Is Imaged. Stroke.
46. Uematsu, H., M. Maeda (2006) Double-echo perfusion-weighted MR imaging: basic concepts and application in brain tumors for the assessment of tumor blood volume and vascular permeability. Eur Radiol. 16(1): 180-6.
47. Gahramanov, S., L.L. Muldoon, X. Li, E.A. Neuwelt (2011) Improved Perfusion MR Imaging Assessment of Intracerebral Tumor Blood Volume and Antiangiogenic Therapy Efficacy in a Rat Model with Ferumoxytol. Radiology. 261(3): 796-804.
48. Barrett, T., M. Brechbiel, M. Bernardo, P.L. Choyke (2007) MRI of tumor angiogenesis. J Magn Reson Imaging. 26(2): 235-49.
49. Tofts, P.S., G. Brix, D.L. Buckley, J.L. Evelhoch, E. Henderson, M.V. Knopp, H.B. Larsson, T.Y. Lee, N.A. Mayr, G.J. Parker, R.E. Port, J. Taylor, R.M. Weisskoff (1999) Estimating kinetic parameters from dynamic contrast-enhanced T(1)-weighted MRI of a diffusable tracer: standardized quantities and symbols. J Magn Reson Imaging. 10(3): 223-32.
50. Li, X., W.D. Rooney, C.G. Varallyay, S. Gahramanov, L.L. Muldoon, J.A. Goodman, I.J. Tagge, A.H. Selzer, M.M. Pike, E.A. Neuwelt, C.S. Springer, Jr. (2010) Dynamic-contrast-enhanced-MRI with extravasating contrast reagent: rat cerebral glioma blood volume determination. J Magn Reson. 206(2): 190-9.
51. Gomori, J.M., R.I. Grossman, H.I. Goldberg, R.A. Zimmerman, L.T. Bilaniuk (1985) Intracranial hematomas: imaging by high-field MR. Radiology. 157(1): 87-93.
52. Gomori, J.M., R.I. Grossman, D.B. Hackney, H.I. Goldberg, R.A. Zimmerman, L.T. Bilaniuk (1988) Variable appearances of subacute intracranial hematomas on high-field spin-echo MR. AJR Am J Roentgenol. 150(1): 171-8.
53. Crawley, A.P., R.M. Henkelman (1988) A comparison of one-shot and recovery methods in T1 imaging. Magn Reson Med. 7(1): 23-34.

54. Nekolla, S., T. Gneiting, J. Syha, R. Deichmann, A. Haase (1992) T1 maps by K-space reduced snapshot-FLASH MRI. J Comput Assist Tomogr. 16(2): 327-32.

55. Neuwelt, E.A., P.E. Guastadisegni, P. Varallyay, N.D. Doolittle (2005) Imaging changes and cognitive outcome in primary CNS lymphoma after enhanced chemotherapy delivery. AJNR Am J Neuroradiol. 26(2): 258-65.

56. Parikh, A.H., J.K. Smith, M.G. Ewend, E. Bullitt (2004) Correlation of MR perfusion imaging and vessel tortuosity parameters in assessment of intracranial neoplasms. Technol Cancer Res Treat. 3(6): 585-90.

57. Kamba, M., Y. Suto, T. Ogawa (1999) Measurement of cerebral mean transit time by dynamic susceptibility contrast magnetic resonance imaging. Eur J Radiol. 31(3): 170-3.

58. Valter, M.M., O.D. Wiestler, T. Pietsche (1999) Differential control of VEGF synthesis and secretion in human glioma cells by IL-1 and EGF. Int J Dev Neurosci. 17(5-6): 565-77.

59. Claes, A., G. Gambarota, B. Hamans, O. van Tellingen, P. Wesseling, C. Maass, A. Heerschap, W. Leenders (2008) Magnetic resonance imaging-based detection of glial brain tumors in mice after antiangiogenic treatment. Int J Cancer. 122(9): 1981-6.

60. Wu, Y.J., L.L. Muldoon, D.T. Dickey, S.J. Lewin, C.G. Varallyay, E.A. Neuwelt (2009) Cyclophosphamide enhances human tumor growth in nude rat xenografted tumor models. Neoplasia. 11(2): 187-95.

61. Guney, S., A. Schuler, A. Ott, S. Hoschele, S. Zugel, E. Baloglu, P. Bartsch, H. Mairbaurl (2007) Dexamethasone prevents transport inhibition by hypoxia in rat lung and alveolar epithelial cells by stimulating activity and expression of Na+-K+-ATPase and epithelial Na+ channels. Am J Physiol Lung Cell Mol Physiol. 293(5): L1332-8.

62. Neuwelt, E.A., D.E. Baker, M.A. Pagel, N.K. Blank (1984) Cerebrovascular permeability and delivery of gentamicin to normal brain and experimental brain abscess in rats. J Neurosurg. 61(3): 430-9.

63. de Crespigny, A.J., D. Howard, H. D'Arceuil, H. Muller, A.T. Agoston, S. Seri, Y. Hashiguchi, C. Fujimoto, A. Nakatani, M.E. Moseley (1999) Dynamic

contrast-enhanced MRI of Implanted VX2 tumors in rabbit muscle: comparison of Gd-DTPA and NMS60. Magn Reson Imaging. 17(9): 1297-305.

64. Akeson, P., C.H. Nordstrom, S. Holtas (1997) Time-dependency in brain lesion enhancement with gadodiamide injection. Acta Radiol. 38(1): 19-24.

65. Silbergeld, D.L., M.R. Chicoine (1997) Isolation and characterization of human malignant glioma cells from histologically normal brain. J Neurosurg. 86(3): 525-31.

66. Yano, T., T. Kodama, Y. Suzuki, K. Watanabe (1997) Gadolinium-enhanced 3D time-of-flight MR angiography. Experimental and clinical evaluation. Acta Radiol. 38(1): 47-54.

67. Bremer, C., M. Mustafa, A. Bogdanov, Jr., V. Ntziachristos, A. Petrovsky, R. Weissleder (2003) Steady-state blood volume measurements in experimental tumors with different angiogenic burdens a study in mice. Radiology. 226(1): 214-20.

68. Cao, Y., C.I. Tsien, V. Nagesh, L. Junck, R. Ten Haken, B.D. Ross, T.L. Chenevert, T.S. Lawrence (2006) Clinical investigation survival prediction in high-grade gliomas by MRI perfusion before and during early stage of RT. Int J Radiat Oncol Biol Phys. 64(3): 876-85.

69. Pike, M., C.P. Langford, C. Neumann, L. Nabors, G. Gillespie. Assessment of mouse glioma vasculature using SPIO and small molecule contrast agents: sequential implementation of alternate perfusion MRI methodologies. in ISMRM 2006.

70. Bastin, M.E., T.K. Carpenter, P.A. Armitage, S. Sinha, J.M. Wardlaw, I.R. Whittle (2006) Effects of dexamethasone on cerebral perfusion and water diffusion in patients with high-grade glioma. AJNR Am J Neuroradiol. 27(2): 402-8.

71. Leenders, K.L., R.P. Beaney, D.J. Brooks, A.A. Lammertsma, J.D. Heather, C.G. McKenzie (1985) Dexamethasone treatment of brain tumor patients: effects on regional cerebral blood flow, blood volume, and oxygen utilization. Neurology. 35(11): 1610-6.

72. Ostergaard, L., F.H. Hochberg, J.D. Rabinov, A.G. Sorensen, M. Lev, L. Kim, R.M. Weisskoff, R.G. Gonzalez, C. Gyldensted, B.R. Rosen (1999) Early

changes measured by magnetic resonance imaging in cerebral blood flow, blood volume, and blood-brain barrier permeability following dexamethasone treatment in patients with brain tumors. J Neurosurg. 90(2): 300-5.

73. Gambarota, G., W. Leenders, C. Maass, P. Wesseling, B. van der Kogel, O. van Tellingen, A. Heerschap (2008) Characterisation of tumour vasculature in mouse brain by USPIO contrast-enhanced MRI. Br J Cancer. 98(11): 1784-9.

11 BIBLIOGRAPHY – list of own publications

11.1 Publications related to the thesis

1. Neuwelt EA, Varallyay CG, Manninger S, Solymosi D, Haluska M, Hunt MA, Nesbit G, Stevens A, Jerosch-Herold M, Jacobs PM, Hoffman JM. The potential of ferumoxytol nanoparticle magnetic resonance imaging, perfusion, and angiography in central nervous system malignancy: a pilot study. ***Neurosurgery*** **60:**(4) *pp. 601-611.* (2007) IF: 3.007

2. Varallyay CG, Muldoon LL, Gahramanov S, Wu YJ, Goodman JA, Li X, Pike MM, Neuwelt EA. Dynamic MRI using iron oxide nanoparticles to assess early vascular effects of antiangiogenic versus corticosteroid treatment in a glioma model. ***J Cereb Blood Flow Metab*** **29:**(4) *pp. 853-860.* (2009) IF: 5.457

3. Weinstein JS, Varallyay CG, Dosa E, Gahramanov S, Hamilton B, Rooney WD, Muldoon LL, Neuwelt EA. Superparamagnetic iron oxide nanoparticles: diagnostic magnetic resonance imaging and potential therapeutic applications in neurooncology and central nervous system inflammatory pathologies, a review. ***J Cereb Blood Flow Metab*** **30:**(1) *pp. 15-35.* (2010) IF: 4.522

4. Neuwelt EA, Hamilton BE, Varallyay CG, Rooney WR, Edelman RD, Jacobs PM, Watnick SG. Ultrasmall superparamagnetic iron oxides (USPIOs): a future alternative magnetic resonance (MR) contrast agent for patients at risk for nephrogenic systemic fibrosis (NSF)? ***Kidney Int*** **75:**(5) *pp. 465-474.* (2009) IF: 6.193

5. Gahramanov S, Raslan AM, Muldoon LL, Hamilton BE, Rooney WD, Varallyay CG, Njus JM, Haluska M, Neuwelt EA. Potential for differentiation of pseudoprogression from true tumor progression with dynamic susceptibility-weighted contrast-enhanced magnetic resonance imaging using ferumoxytol vs. gadoteridol: a pilot study. ***Int J Radiat Oncol Biol Phys*** **79:**(2) *pp. 514-523.* (2011) IF: 4.503*

11.2 Further scientific publications

1. Doolittle ND, Jahnke K, Belanger R, Ryan DA, Nance RW Jr, Lacy CA, Tyson RM, Haluska M, Hedrick NA, Varallyay C, Neuwelt EA. Potential of chemo-immunotherapy and radioimmunotherapy in relapsed primary central nervous system (CNS) lymphoma. ***Leuk Lymphoma*** **48:**(9) *pp. 1712-1720.* (2007) IF: 1.512

2. Várallyay Cs, Balázs Gy, Lénárd Zs, Bérczi V, Belics Z, Bajzik G, Wragg P, Hüttl, Kálmán, Jolesz, Ferenc A. MR imaging follow up after MR-guided focused ultrasound surgery for uterine leiomyomas.: Early and mid term results. ***Interventional Medicine & Applied Science*** **1:**(1) *pp. 46-51.* (2009)

3. Berczi V, Molnar AA, Apor A, Kovacs V, Ruzics C, Varallyay C, Huttl K, Monos E, Nadasy GL. Non-invasive assessment of human large vein diameter, capacity, distensibility and ellipticity in situ: dependence on anatomical location, age, body position and pressure. ***Eur J Appl Physiol*** **95:**(4) *pp. 283-289.* (2005) IF: 1.619

4. Li X, Rooney WD, Varallyay CG, Gahramanov S, Muldoon LL, Goodman JA, Tagge IJ, Selzer AH, Pike MM, Neuwelt EA, Springer CS Jr. Dynamic-contrast-enhanced-MRI with extravasating contrast reagent: rat cerebral glioma blood volume determination. ***J Magn Reson*** **206:**(2) *pp. 190-199.* (2010) IF: 2.333

5. Wu YJ, Muldoon LL, Varallyay C, Markwardt S, Jones RE, Neuwelt EA. In vivo leukocyte labeling with intravenous ferumoxides/protamine sulfate complex and in vitro characterization for cellular magnetic resonance imaging. ***Am J Physiol Cell Physiol*** **293:**(5) *pp. C1698-C1708.* (2007) IF: 4.230

6. Jahnke K, Muldoon LL, Varallyay CG, Lewin SJ, Brown RD, Kraemer DF, Soussain C, Neuwelt EA. Efficacy and MRI of rituximab and methotrexate treatment in a nude rat model of CNS lymphoma. ***Neuro Oncol*** **11:**(5) *pp. 503-513.* (2009) IF: 4.984

7. Jahnke K, Muldoon LL, Varallyay CG, Lewin SJ, Kraemer DF, Neuwelt EA. Bevacizumab and carboplatin increase survival and asymptomatic tumor volume in a glioma model. ***Neuro Oncol*** **11:**(2) *pp. 142-150.* (2009) IF: 4.984

8. Wu YJ, Muldoon LL, Dickey DT, Lewin SJ, Varallyay CG, Neuwelt EA. Cyclophosphamide enhances human tumor growth in nude rat xenografted tumor models. ***Neoplasia*** **11:**(2) *pp. 187-195.* (2009) IF: 5.025

9. Soussain C, Muldoon LL, Varallyay C, Jahnke K, DePaula L, Neuwelt EA. Characterization and magnetic resonance imaging of a rat model of human B-cell central nervous system lymphoma. ***Clin Cancer Res*** **13:**(8) *pp. 2504-2511.* (2007) IF: 6.250

12 ACKNOWLEDGEMENT

First of all I would like to thank to all my coworkers at the OHSU BBB program, including administrative personnel, laboratory assistants, my researcher colleagues, and finally the head of this program, Edward Neuwelt. Also, I am grateful to Charles Springer, the director of the Advanced Imaging Research Center at OHSU, and all the people, who made possible those hundreds, or thousands of MRI scans. Special thanks to Kálmán Hüttl, Viktor Bérczi, György Balázs and many further employees of the Semmelweis University for their support throughout my PhD Studies. Finally I would like to show my appreciation to Edit Dósa, and László Szidonya for their critical review, showing the right track in finalizing this work.

12.1 Conflict of interest:

The studies were entirely funded by the Veterans Administration and the National Institute of Health research grants, with the ferumoxytol USPIO nanoparticles donated by AMAG pharmaceuticals. In light of the results from this study, OHSU has received a sponsored research agreement from AMAG to conduct clinical trials of MRI with ferumoxytol. None of the authors has financial interest in this agent or in its developer AMAG.